summer 2019: No. 11

gacm German Association for Computational Mechanics

Report

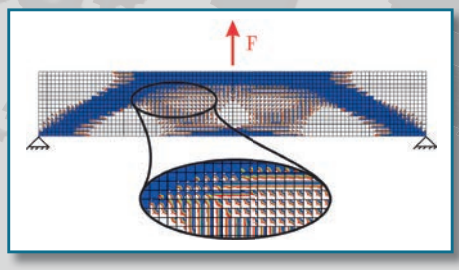

Thermodynamic extremal principles for topology optimization

Philipp Junker, Dustin R. Jantos

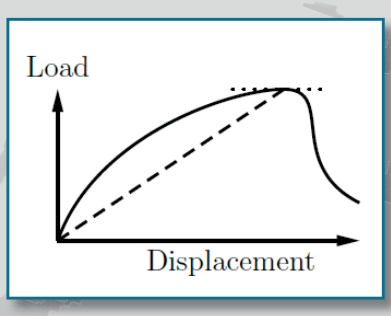

Topology optimization beyond linear elasticity

Mathias Wallin, Daniel Tortorelli

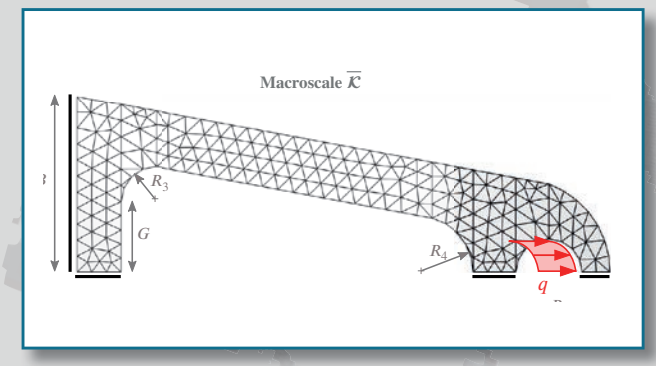

Variational design sensitivity analysis and multiscale optimisation

Franz-Joseph Barthold, Wojciech Kijanski

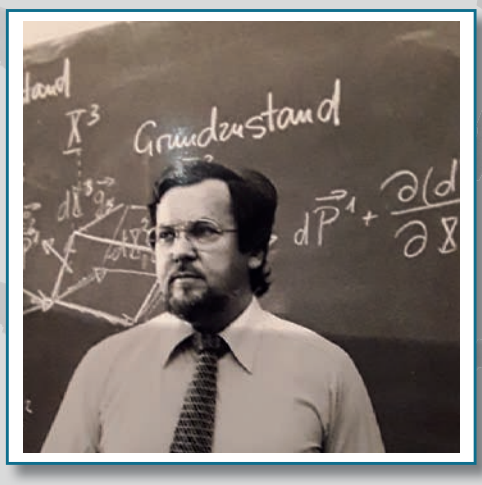

In Memoriam Erwin Stein (1931 – 2018)

Walter Wunderlich

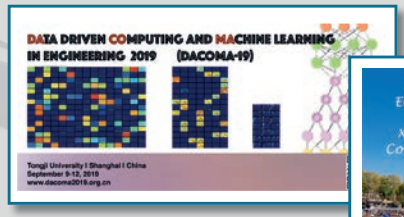

Conferences

8th ECCOMAS Congress & 14th WCCM 2020

AfriComp 2020/SACAM 2020

DACOMA-19

contents

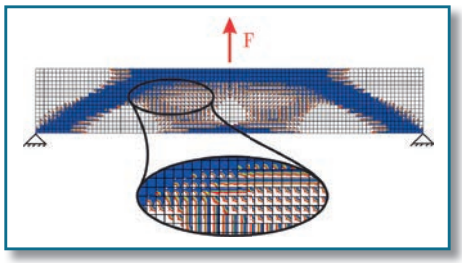

GACM-NEWS

Journal

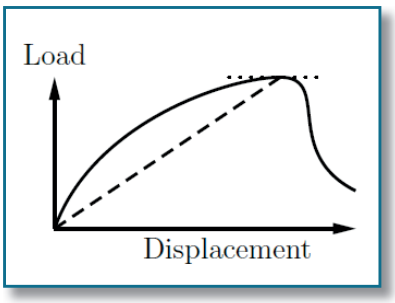

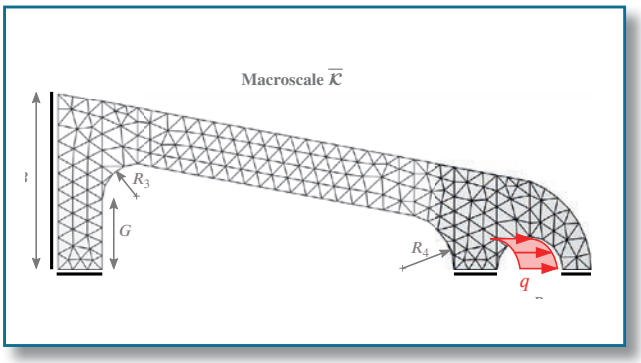

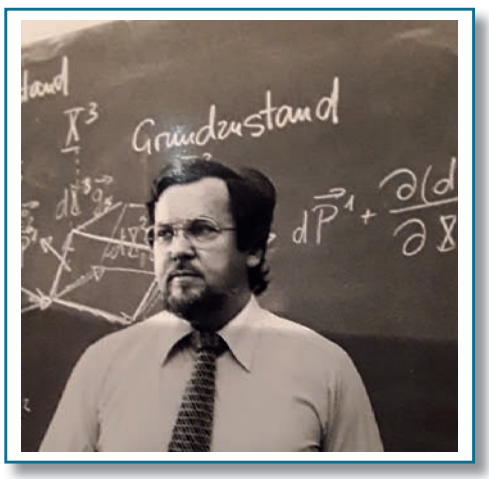

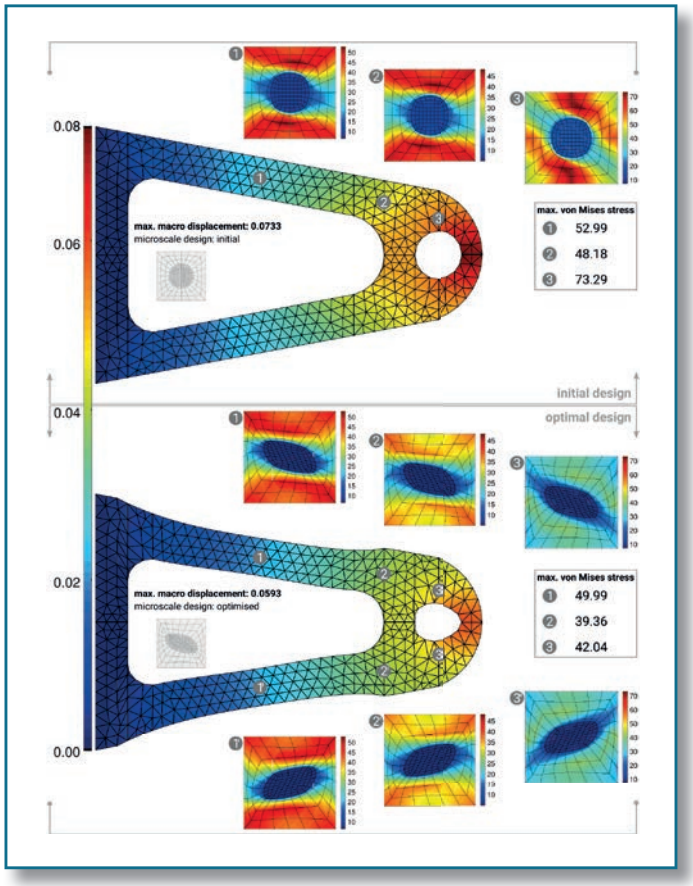

Conferences

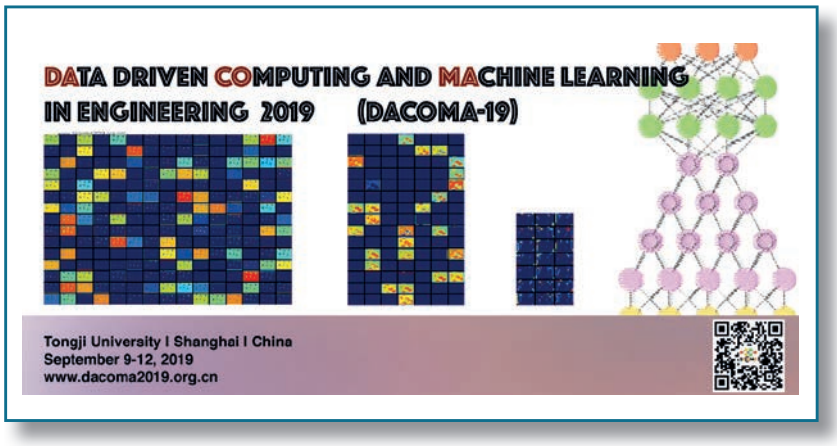

gacm German Association for Computational Mechanics

Publisher:
GACM
The German Association for Computational Mechanics

Address:
Institut für Statik und Dynamik der Tragwerke
Technische Universität Dresden
01062 Dresden
Phone: +49 351-463-35738
Fax: +49 351-463-37086
email: gacm@mailbox.tu-dresden.de
Internet: www.gacm.de

Editor-in-Chief: Michael Kaliske

Guest Editor: Andreas Menzel, Richard Ostwald

Grafik-Design & Print:
K. Schmidle Druck und Medien GmbH, Ebersberg

Print Run: 530

Editorial

This issue of the GACM Report highlights current developments in the field of topology optimization, with a particular focus on the challenges arising in the context of materially non-linear, dynamic, and multiscale optimization problems. To this end, three articles are presented in this issue, each focussing on particular features of modern topology optimization procedures.

The article **Thermodynamic extremal principles for topology optimization** by Philipp Junker and Dustin R. Jantos solves the inverse problem of topology optimization by application of thermodynamic extremal principles – a common tool in continuum mechanics for the modelling of physically sound non-linear material behaviour. The article highlights the fact that thermodynamic extremal principles for topology optimization can be directly combined with established principles for material modelling, thus enabling a natural inclusion of material non-linearities in the topology optimization procedure.

The contribution **Topology optimization beyond linear elasticity** by Mathias Wallin and Daniel Tortorelli discusses current developments not only with respect to the inclusion of material non-linearities, but also with respect to the inclusion of dynamic effects in the context of topology optimization tasks. To this end, the article provides representative numerical examples, including topology optimization examples in the context of non-linear elasticity, finite deformation plasticity, and dynamic problems.

Finally, the article **Variational Design Sensitivity Analysis and Multiscale Optimisation** by Franz-Joseph Barthold and Wojciech Kijanski focusses on the application of optimization principles to multi-scale problems. The FE^2 approach is a commonly used method for the modelling of multi-scale materials, facilitating the consideration of material inhomogeneities on the micro-scale via representative volume elements. The presented article combines FE^2 based multi-scale analyses with a multi-scale structural optimization method for the monolithic computation of optimal micro- and macro-scale layouts.

On behalf of GACM, we would like to express our gratitude to the above named authors for presenting the current activities and developments in the challenging and complex field of non-linear, dynamic, and multi-scale topology optimization problems in this issue.

March 2019

Andreas Menzel
Institute of Mechanics
TU Dortmund University
Division of Solid Mechanics
Lund University

Richard Ostwald
Bremen Institute of Mechanical Engineering
University of Bremen
Institute of Mechanics
TU Dortmund University

Message of the President

The German Association for Computational Mechanics (GACM) is pleased to provide this GACM-Report No. 11. The initiative of guest editors Professor Andreas Menzel and Interim Professor Richard Ostwald is especially acknowledged. The topics addressed out of the field of optimization are of significant importance and play a major role in the context of virtual product development.

At the end of the year 2018, the scientific community learned with great sadness that Professor Erwin Stein passed away. He was Honorary President of GACM and an outstanding, passionate scientist. Professor Walter Wunderlich, his long-time colleague and friend, recalls in a very personal obituary aspects of the life of Professor Stein.

The combined 8th ECCOMAS Congress and 14th World Congress on Computational Mechanics will take place 19 to 24 July 2020 in Paris. This mega-event is already under busy preparation. GACM plays as co-organiser a substantial role in supporting the French colleagues in their preliminary activities. The German community for computational mechanics is encouraged to contribute heavily to this eminent conference. Moreover, the next general assembly of GACM will be held in Paris during this event.

Professor Zhuo Zhuang, the president of the Chinese partner association CACM, expressed the strong wish to interact with GACM more intensively. A first step to have common activities is the international conference on Data Driven Computing and Machine Learning in Engineering 2019 (DACOMA-19), which will be held in Shanghai 9 to 11 September this year. This conference is supported by CACM and GACM.

A central and important gathering is the 8th GACM Colloquium on Computational Mechanics, which will be organized on 28 to 30 August this year in Kassel. The GACM Colloquium intends to bring together especially young scientists, who are engaged in academic as well as in industrial research on computational mechanics and computer methods in applied sciences. This series of conferences is a great success story in its category.

This year, the thematic conferences under the roof of ECCOMAS take place. Quite a number of these conferences are organized in Germany:

- CFRAC 2019: Sixth International Conference on Computational Modeling of Fracture and Failure of Materials and Structures, 12-14 June, Braunschweig,
- M-FET 2019: 2nd Modern Finite Element Technologies - Mathematical and Mechanical Aspects, 01-03 July, Bad Honnef,
- ICCCM 2019: International Conference on Computational Contact Mechanics, 03-05 July, Hannover,
- MULTIBODY 2019: Multibody Dynamics, 15-18 July, Duisburg,
- IGA 2019: VII International Conference on Isogeometric Analysis, 18-20 September, Munich,
- ICBT 2019: III International Conference on Biomedical Technology, 18-20 November, Hannover.

The commitment to provide these important scientific conferences creates good visibility of our national community.

Another interesting conference will be SACAM 2020, which is combined with AfriComp 2020, organised by the South African mechanics community at Cape Town on 30 November to 2 December 2020. GACM supports explicitly this conference in order to foster computational mechanics research in Africa.

Finally, I would like to point out that on 21 October 2019 until 18 November 2019 elections for the Review Boards (Fachkollegien) for Deutsche Forschungsgemeinschaft (DFG) will take place. Every eligible voter in our scientific system is strongly encouraged to take part in these elections in order to determine the persons who shall represent the interests of the scientific community within the DFG. The nominated candidates will be announced this summer.

Looking forward towards the upcoming scientific events and I remain with my best regards

Michael Kaliske, President of GACM

Thermodynamic extremal principles for topology optimization

by Philipp Junker[1] and Dustin R. Jantos[1]

[1]Mechanik – Materialtheorie, Ruhr-Universität Bochum, Germany

Abstract

Thermodynamic extremal principles constitute a prominent tool for material modeling. However, it turned out that these principles cover an even broader range of applicability. To be more precise, the so-called inverse problem of topology optimization can also be investigated and solved in an elegant manner by application of thermodynamic extremal principles. Due to their origin in material modeling, the inclusion of material nonlinearities to topology optimization can be performed in a straightforward manner.

Introduction

The idea of describing processes that are observed in nature by extremal principles roots back to Aristotle or even earlier (see [4]). The popular principle of least action follows from this fundamental modeling strategy, which was successfully applied to the problem of brachistochrone, light refraction, the motion of a conservative oscillator, and many more. The appropriate mathematical theory was established in the late 1700s by Leibniz, Euler, Maupertuis, Lagrange, and others. See [42] for a historical review and the investigation of the principle of Castigliano and Menabrea in [6], which constitutes as a special case of the principle of least action. A more general formulation of the principle of least action is the Hamilton principle [15, 16], of which a didactic presentation can be found in [2].

The Hamilton principle can be formulated for conservative continua as

$$\delta\mathcal{G} = \delta\mathcal{K} \quad \forall\delta\boldsymbol{u} \ , \tag{1}$$

where $\mathcal{K}$ denotes the kinetic energy and $\mathcal{G}$ the Gibbs energy. The Gâteaux derivative is indicated by a preceding δ, and $\boldsymbol{u}$ denotes the displacements. The Gibbs energy is given by

$$\mathcal{G} = \int_\Omega \Psi \ \mathrm{d}V - \int_\Omega \boldsymbol{f}\cdot\boldsymbol{u} \ \mathrm{d}V - \int_{\partial\Omega} \boldsymbol{t}\cdot\boldsymbol{u} \ \mathrm{d}A \tag{2}$$

with the Helmholtz free energy Ψ, the volume forces $\boldsymbol{f}$, and the tractions $\boldsymbol{t}$. The volume of the body is indicated by Ω and the boundary by $\partial\Omega$, respectively. For modeling of nonconservative continua, i.e. evolving microstructures, appropriate internal variables $\boldsymbol{v}$ are introduced. This evolution contributes to the Hamilton principle, such that it reads (for the quasistatic case, i.e. $\delta\mathcal{K} = 0$)

$$\delta\mathcal{G} = \delta\mathcal{D} \quad \forall\delta\boldsymbol{u},\, \delta\boldsymbol{v} \ , \tag{3}$$

which is also referred to as the principle of virtual work. The nonconservative microstructural evolution enters the Hamilton principle by means of the dissipation functional

$$\mathcal{D} := \int_\Omega \hat{\boldsymbol{p}}\cdot\delta\boldsymbol{v} \ \mathrm{d}V \ , \tag{4}$$

in which $\hat{\boldsymbol{p}}$ denotes the nonconservative forces acting along the "distance of microstructure evolution" $\delta\boldsymbol{v}$. Without loss of generality, it might be assumed that these forces can be derived from a dissipation potential $\Delta = \Delta(\boldsymbol{v}, \dot{\boldsymbol{v}})$ such that

$$\hat{\boldsymbol{p}} := -\frac{\partial\Delta}{\partial\dot{\boldsymbol{v}}} \tag{5}$$

holds. Consequently, the Hamilton principle can be formulated as

$$\delta\mathcal{G} + \int_\Omega \frac{\partial\Delta}{\partial\dot{\boldsymbol{v}}}\cdot\delta\boldsymbol{v} \ \mathrm{d}V = 0 \ \forall\delta\boldsymbol{u},\, \delta\boldsymbol{v} \ . \tag{6}$$

A great benefit of this variational strategy is the easy inclusion of (complex) constraints by adding appropriate energetic functionals. For the case of vanishing gradients of the internal variable, i.e. $\mathcal{G} = \mathcal{G}[\boldsymbol{u}, \nabla^{\mathrm{s}}\boldsymbol{u}, \boldsymbol{v}]$, the stationarity condition in Eq. (6) with respect to $\delta\boldsymbol{v}$ becomes

$$\frac{\partial\Delta}{\partial\dot{\boldsymbol{v}}} = -\frac{\partial\Psi}{\partial\boldsymbol{v}} =: \boldsymbol{p} \ , \tag{7}$$

which is known as Biot equation, c.f. [5]. For adequate choices of the dissipation function Δ, e.g. Δ being homogeneous of first or second order, Eq. (7) coincides with Onsager's principle [38, 39]

$$\dot{\boldsymbol{v}} \propto \boldsymbol{p} \tag{8}$$

with the thermodynamic fluxes $\dot{\boldsymbol{v}}$ and the thermodynamic driving forces $\boldsymbol{p}$, respectively. Consequently, all material models derived by the use of thermodynamic extremal principles identically fulfill the second law of thermodynamics

$$-\frac{\partial\Psi}{\partial\boldsymbol{v}}\cdot\dot{\boldsymbol{v}} = \boldsymbol{p}\cdot\dot{\boldsymbol{v}} \geq 0 \ . \tag{9}$$

A potential form of the Biot equation is given by

$$\Lambda = \dot{\Psi} + \Delta \to \min_{\dot{\boldsymbol{v}}} \ , \tag{10}$$

which is referred to as the principle of the minimum of the dissipation potential, cf. [7, 25]. A comparable approach is the principle of maximum dissipation, e.g. [13, 14]. It is also possible to formulate the thermodynamic extremal principles in a time-discrete way, cf. [40, 34, 35, 37].

These modeling strategies have been successfully applied to various problems of material modeling, e.g. phase transformations [36, 24], crystal plasticity [29], and damage [33, 31], to mention just a few. Based on the idea of an "inverse" damage model, which redistributes mass from low to highly loaded parts in a design space, the thermodynamic topology optimization has been derived using the very same thermodynamic extremal principles [22, 23, 18, 19]. The fundamental idea, regularization approaches, inclusion of material nonlinearities and several numerical examples are presented in the following.

Fundamentals

The application of the thermodynamic extremal principles discussed in the previous section requires postulation of the Helmholtz free energy and the dissipation function; whereas the latter basically determines the type of the resulting evolution equation. For the modeling of damage processes, several approaches make use of a Helmholtz free energy as

$$\Psi_{\mathrm{d}} = \frac{1}{2}\boldsymbol{\varepsilon} : f(d)\mathbb{E} : \boldsymbol{\varepsilon} \ , \tag{11}$$

where ε denote the strains and $\mathbb{E}$ the fourth-order elasticity tensor. The interpolation between the undamaged and the damaged material is described by means of the interpolation function $f(d)$ with the damage parameter d as internal variable. Examples can be found, e.g., in [10, 12, 26]. This fundamental idea of interpolation between high and low (local) stiffness can also be applied to topology optimization [22], simply by formulating

$$\Psi = \Psi_{\mathrm{m}} = \frac{1}{2}\boldsymbol{\sigma} : [f(\chi)\mathbb{E}]^{-1} : \boldsymbol{\sigma} \ . \tag{12}$$

In contrast to strain-controlled damage processes, the control variable in topology optimization is the mechanical stress. The internal variable $\chi \in [\chi_{\min}, 1]$ serves as design variable, such that the local (relative) density is given by $f(\chi)$. Various approaches for the interpolation function are possible, for example $f(\chi) = \chi_{\min}(\chi_{\min} - 1)/[\chi_{\min}(\chi_{\min} - 1) - (\chi - 1)^2]$ in [22] or $f(\chi) = \chi^3$ and $\chi_{\min} = 10^{-3}$ in [17].

The dissipation function is chosen as

$$\Delta = \frac{1}{2}\eta\dot{\chi}^2 \ , \tag{13}$$

which results in an evolution equation of viscous type, cf. [18]. The quantity η is the viscosity. The ansatz $\tilde{\Delta} = \Delta + r|\dot{\chi}|$ yields an evolution of an elasto-viscoplastic type, cf. [22, 23]. The interval constraint for the design variable χ is accounted for by a Kuhn-Tucker parameter

$$\gamma = \begin{cases} \tilde{\gamma} & : \quad \dot{\chi} > 0 \wedge \chi = 1 \\ -\tilde{\gamma} & : \quad \dot{\chi} < 0 \wedge \chi = \chi_{\min} \\ 0 & : \quad \text{else} \ . \end{cases} \tag{14}$$

Furthermore, we also have to control the total mass in the design volume $\varrho\Omega$, which results in the constraint

$$\int_\Omega g(\chi) \ \mathrm{d}V - \varrho\Omega = 0 \tag{15}$$

that is accounted for via a Lagrange parameter λ. Consequently, a functional for the constraints is formulated as

$$\mathcal{C}_\chi = \int_\Omega \gamma\chi \ \mathrm{d}V + \lambda\left(\int_\Omega g(\chi) \ \mathrm{d}V - \rho\Omega\right) \ . \tag{16}$$

Several approaches for the function $g(\chi)$ are possible, e.g. $g(\chi) = 1/f(\chi)$ in [18] or $g(\chi) = \chi$ in [17]. This allows us to apply the Hamilton principle as

$$\delta\mathcal{G} + \int_\Omega \frac{\partial\Delta}{\partial\dot{\chi}}\delta\chi \ \mathrm{d}V + \int_\Omega \gamma\delta\chi \ \mathrm{d}V + \lambda\int_\Omega g'(\chi)\delta\chi \ \mathrm{d}V = 0 \quad \forall\delta\boldsymbol{u}, \ \delta\chi \ . \tag{17}$$

Evaluation of the stationarity condition with respect to χ results for fixed stresses in the evolution equation

$$0 = -p + \eta\dot{\chi} + \gamma + \lambda g' \tag{18}$$

with the thermodynamic driving force $p := -\partial\Psi/\partial\chi$. In contrast to classical approaches to topology optimization, see e.g. [3, 8, 43], the update of the design variable is described in terms of an ODE, referred to as evolution equation in the context of material modeling. A comparable structure results when approaches for dynamical systems are applied [27, 28].

The evolution equation (18) can be compared to growth modeling, cf. [30, 46]. However, a major difference is that nonlinear interpolation functions $f(\chi)$ are used for topology optimization, which results in a nonconvex Helmholtz free energy Ψ. A first numerical example is given in Fig. 1, cf. [23]. The nonconvex Helmholtz free energy results in a "black/white" solution, i.e. no large "gray" areas with $\chi \in]0, 1[$ are present. However, the evaluation of a nonconvex and unregularized energy results in severe numerical issues in a finite-element implementation: void and full material fluctuate periodically. This phenomenon is widely known: in the context of damage modeling, the localization results in undesired mesh-dependencies, see e.g. [10], whereas the periodicity in topology optimization is referred to as the checkerboard phenomenon [44]. Consequently, an appropriate regularization is required.

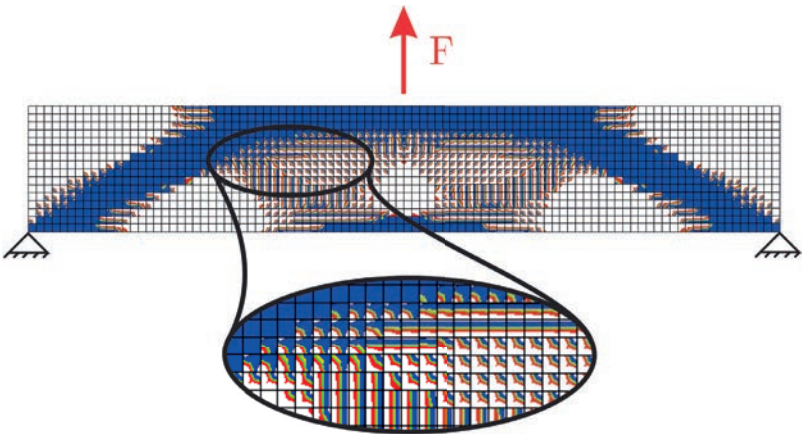

Figure 1: Numerical result for an implementation of Eq. (18) via a material model interface into a finite-element code.

Regularization

Classically, filters are used for regularization and to thus suppress the checkerboarding, cf. [44, 47]. However, instead of using (heuristic) filter techniques, it is also possible to apply regularization schemes from material modeling, which render the problem well-posed. For instance, gradient enhancement known from damage modeling [9] or localized phase transformations [21] can be employed. To this end, the Helmholtz free energy in Eq. (12) is expanded by terms for regularization, viz.

$$\Psi = \Psi_{\mathrm{m}} + \Psi_{\mathrm{r}} = \frac{1}{2}\boldsymbol{\sigma} : [f(\chi)\mathbb{E}]^{-1} : \boldsymbol{\sigma} + \frac{1}{2}c_1(\varphi-\chi)^2 + \frac{1}{2}c_2|\nabla\varphi|^2 \ , \tag{19}$$

with some parameters c_1 and c_2. The Hamilton principle then reads

$$\delta\mathcal{G} + \int_\Omega \frac{\partial\Delta}{\partial\dot{\chi}}\delta\chi \ \mathrm{d}V + \int_\Omega \gamma\delta\chi \ \mathrm{d}V + \lambda\int_\Omega g'(\chi)\delta\chi \mathrm{d}V = 0 \ \forall\delta\boldsymbol{u},\ \delta\varphi,\ \delta\chi \ . \tag{20}$$

The respective variations $\delta\boldsymbol{u}$, $\delta\varphi$, and $\delta\chi$ can be chosen arbitrarily. Thus, the stationarity conditions are evaluated separately, yielding

$$\int_\Omega \frac{\partial\Psi}{\partial\boldsymbol{\varepsilon}} : \delta\boldsymbol{\varepsilon} \ \mathrm{d}V - \int_\Omega \boldsymbol{f}\cdot\delta\boldsymbol{u} \ \mathrm{d}V - \int_{\partial\Omega} \boldsymbol{t}\cdot\delta\boldsymbol{u} \ \mathrm{d}A = 0 \qquad \forall\delta\boldsymbol{u} \tag{21}$$

$$\int_\Omega c_1(\varphi-\chi)\delta\varphi \ \mathrm{d}V + \int_\Omega c_2\nabla\varphi\cdot\nabla\delta\varphi \ \mathrm{d}V = 0 \qquad \forall\delta\varphi \tag{22}$$

$$-p_{\mathrm{m}} + \eta\dot{\chi} + \gamma + \lambda - c_1(\varphi-\chi) = 0 \tag{23}$$

with $p_{\mathrm{m}} := -\partial\Psi_{\mathrm{m}}/\partial\chi$. The first equation is nothing else but the weak form of the balance of linear momentum with $\partial\Psi/\partial\boldsymbol{\varepsilon} \equiv \boldsymbol{\sigma}$. The gradient enhancement regularizes the evolution of the design variable via the last term $c_1(\varphi-\chi)$ in Eq. (23). Equations (21) and (22) can be solved using the finite-element method, which transforms them into a system of algebraic equations with the nodal unknowns $\boldsymbol{u}$ and φ. For a complete derivation and details of the numerical treatment, we refer to the original work in [22]. As can be seen in Fig. 2, the gradient enhancement successfully suppresses checkerboarding. However, the increased number of nodal unknowns drastically increases the numerical effort. Consequently, improved regularization strategies are appreciated.

To circumvent the problem of an ill-posed problem as well as the increased computational costs, the results for the unregularized model are investigated. Due to the evaluation of the evolution equation at the integration (=Gauß) points, the checkerboard takes place *intra*-elementarily, cf. Fig. 1. Thus, a numerically advantageous approach for regularization has been proposed in [23]. Here, the gradient is penalized directly, such that the Helmholtz free energy reads

$$\Psi = \Psi_{\mathrm{m}} + \Psi_{\mathrm{r}} = \frac{1}{2}\boldsymbol{\sigma} : [f(\chi)\mathbb{E}]^{-1} : \boldsymbol{\sigma} + \frac{1}{2}\beta|\nabla\chi|^2 \ . \tag{24}$$

Consequently, the Hamilton principle requires evaluation of the stationarity conditions with respect to the displacements and the design variable. The stationarity with respect to the displacement again yields the balance of linear momentum, as given in Eq. (21). However, the stationarity con-

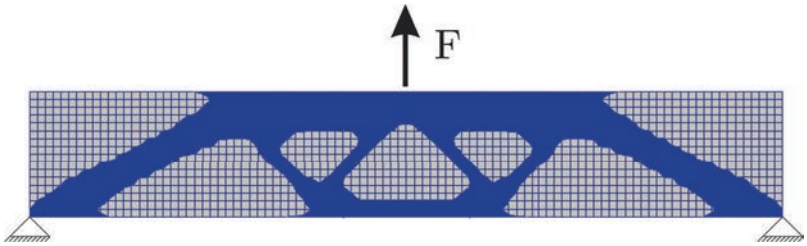

Figure 2: Numerical result for an implementation of the regularized model according to Eqs. (21) to (23).

dition for the design variable yields

$$\int_\Omega \left(-p_\mathrm{m} + \eta\dot{\chi} + \gamma + \lambda\right)\delta\chi \, \mathrm{d}V + \int_\Omega \beta\nabla\chi\cdot\nabla\delta\chi \, \mathrm{d}V = 0 \quad \forall\delta\chi \, , \tag{25}$$

which can be solved in various ways. One possibility was proposed in [23] that makes use of a discontinuous Galerkin method, i.e. the shape functions for χ are defined as

$$N_\chi(\xi_1,\xi_2,\xi_3) \in \left\{\frac{3\sqrt{3}}{8}\left(\frac{1}{\sqrt{3}}\pm\xi_1\right)\left(\frac{1}{\sqrt{3}}\pm\xi_2\right)\left(\frac{1}{\sqrt{3}}\pm\xi_3\right)\right\} \, , \tag{26}$$

with the natural coordinates ξ_i. The special property of these shape functions is

$$(N_\chi(\boldsymbol{\xi}))_i = \begin{cases} 1 & : \boldsymbol{\xi} = \boldsymbol{\xi}_{\mathrm{GP},j} \wedge j = i \\ 0 & : \boldsymbol{\xi} = \boldsymbol{\xi}_{\mathrm{GP},j} \wedge j \neq i \end{cases} \tag{27}$$

with the usual Gauß points $\boldsymbol{\xi}_{\mathrm{GP},j} \in \{(\pm1,\pm1,\pm1)/\sqrt{3}\}$, $j \in \{1,8\}$. Using these discontinuous shape functions and employing an explicit Euler scheme for the time integration reduces the integral equation Eq. (25) to a usual material point law, reading

$$0 = -p_\mathrm{m} + \eta\frac{\chi^{n+1}-\chi^n}{\Delta t} + \gamma + \lambda + \overline{\Delta\chi}_i \tag{28}$$

with the intra-element gradient term

$$\overline{\Delta\chi}_i := \frac{1}{\det J_e}\Big(\int_{\Omega_e} \beta\left(\nabla\boldsymbol{N}_\chi\right)^T\cdot \left(\nabla\boldsymbol{N}_\chi\cdot\boldsymbol{\chi}\right) \, \mathrm{d}V\Big)_i \, . \tag{29}$$

The index i refers to the ith component of the resultant vector, Ω_e indicates the respective element volume, and $\boldsymbol{\chi}$ the nodal vector of the design variable χ in the finite element e. Due to this element-wise evaluation, the displacements remain the only nodal unknowns to be calculated in a monolithic manner. This procedure offers a shorter computation time by one order of magnitude as compared to the model in Eqs. (21) to (23). The discontinuous Galerkin approach is able to compute very complex construction parts, see Fig. 3. However, the intra-element penalization of the gradient of the design variable turns out to be insufficient for more sophisticated problems, e.g. when complex material nonlinearities are to be investigated. Hence, a modified approach that makes use of strategies known for meshless methods, cf. [1, 41], was introduced in [17], which reduces the numerical effort even more and provides direct control over the minimum structure member size, i.e. the minimum diameter of trusses within the structure. The fundamental idea is to work with the strong form of Eq. (25) reading

$$-p_\mathrm{m} + \eta\dot{\chi} + \lambda + \gamma - \beta\nabla^2\chi = 0 \quad \forall x \in \Omega \tag{30}$$

$$\beta\nabla\chi\cdot\boldsymbol{n} = 0 \quad \forall x \in \partial\Omega \tag{31}$$

and to employ an efficient computation of the Laplacean, referred to as the neighbored-element method. To this end, we first apply an element-wise discretization of the design variable, i.e. all Gauß points in the same finite element operate with the same value for χ. We then employ a Taylor series expansion of χ around a central element yielding

$$\Delta\chi_j := \chi_j - \chi_c \approx \sum_{k=1}^{3}\Big(\frac{\partial\chi_c}{\partial x_k}\Delta x_{j,k} + \frac{1}{2}\sum_{p=1}^{3}\frac{\partial^2\chi_c}{\partial x_k\partial x_p}\Delta x_{j,k}\Delta x_{j,p}\Big) \, , \tag{32}$$

where χ_c denotes the design variable at the central element. The neighborhood around the central element is defined by $j \in \{n,s,e,w,f,b,o,p,q\}$ with elements in the north, south, east, west, front and back directions. Three additional elements o,p,q are selected such that each of them lies in one of the $n/s/e/w$, $n/s/f/b$, and $e/w/f/b$ "planes", see Fig. 4. The spatial distances between the mid points of the nine elements in the three directions $k \in \{1,2,3\}$, i.e. $\Delta x_{j,k}$, are given by the finite-element discretization and are fixed during the entire computation. Equation (32) can be written in tensorial form as

$$\Delta\boldsymbol{\chi}_c = \boldsymbol{D}\cdot\partial\boldsymbol{\chi}_c \, . \tag{33}$$

The values of χ at each element is known, so are the differences between the values at the central element and those in its neighborhood. These differences are collected for each element in the vector $\Delta\boldsymbol{\chi}_c$. The known

Figure 3: Result for a wheel bearing using the discontinuous Galerkin approach. The centered cylindrical hole is a constraint that can be easily accounted for by defining it not to be included in the design space Ω. Consequently, it is not discretized by the finite-element mesh. All other holes result from the thermodynamic topology optimization.

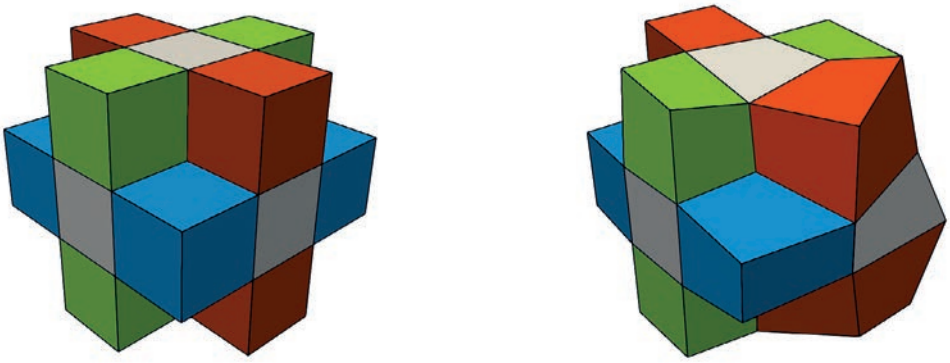

Figure 4: Centered element including its neighborhood for structured (left) and unstructured (right) meshes. The different $n/s/e/w$, $n/s/f/b$, and $e/w/f/b$ "planes" are indicated in red, green, and blue, respectively.

spatial distances are collected in the coefficient matrix $\boldsymbol{D}$

$$\begin{aligned} D_{j,1} &= \Delta x_{j,1} \\ D_{j,2} &= \Delta x_{j,2} \\ D_{j,3} &= \Delta x_{j,3} \\ D_{j,4} &= \Delta x_{j,1}\Delta x_{j,2} \\ D_{j,5} &= \Delta x_{j,1}\Delta x_{j,3} \\ D_{j,6} &= \Delta x_{j,2}\Delta x_{j,3} \\ D_{j,7} &= \frac{(\Delta x_{j,1})^2}{2} \\ D_{j,8} &= \frac{(\Delta x_{j,2})^2}{2} \\ D_{j,9} &= \frac{(\Delta x_{j,3})^2}{2} \,. \end{aligned} \tag{34}$$

The partial derivatives are stored in the vector $\partial\boldsymbol{\chi}_c$

$$\begin{aligned} \partial\boldsymbol{\chi}_c = \Bigg(& \frac{\partial\chi_c}{\partial x_1} \quad \frac{\partial\chi_c}{\partial x_2} \quad \frac{\partial\chi_c}{\partial x_3} \\ & \frac{\partial^2\chi_c}{\partial x_1\partial x_2} \quad \frac{\partial^2\chi_c}{\partial x_1\partial x_3} \quad \frac{\partial^2\chi_c}{\partial x_2\partial x_3} \\ & \frac{\partial^2\chi_c}{\partial x_1^2} \quad \frac{\partial^2\chi_c}{\partial x_2^2} \quad \frac{\partial^2\chi_c}{\partial x_3^2} \Bigg)^{\mathrm{T}} \,. \end{aligned} \tag{35}$$

These spatial derivatives are the unknowns in Eq. (33) and can be computed directly by

$$\partial\boldsymbol{\chi}_c = \boldsymbol{D}^{-1}\cdot\Delta\boldsymbol{\chi}_c \tag{36}$$

Defining the operator matrix $\boldsymbol{B}^{\nabla^2}$ by

$$\begin{aligned} B^{\nabla^2}_{l,j} := D^{-1}_{l+6,j} \,, \quad & l\in\{1,2,3\} \,, \\ & j\in\{1,\dots,9\} \,, \end{aligned} \tag{37}$$

allows us to estimate only the requested unmixed second derivatives collected in a vector by

$$\boldsymbol{B}^{\nabla^2}\cdot\Delta\boldsymbol{\chi}_c = \frac{\partial^2\chi_c}{\partial x_l^2}\boldsymbol{e}_l \,, \quad l\in\{1,2,3\} \,. \tag{38}$$

The required Laplace operator for each element c is then given by

$$(\Lambda_\chi)_c = \sum_{l=1}^{3}\left(\boldsymbol{B}^{\nabla^2}\cdot\Delta\boldsymbol{\chi}_c\right)_l \,. \tag{39}$$

To summarize, the spatial distances are given by the fixed finite-element mesh, implying that $\boldsymbol{D}$ is constant during the entire process of topology optimization. Thus, we can compute the inverse of $\boldsymbol{D}$ and consequently $\boldsymbol{B}^{\nabla^2}$ once in advance for each finite-element mesh. Multiplication of $\boldsymbol{B}^{\nabla^2}$ with the (evolving) spatial differences of the design variables yields the vector of unmixed second derivatives that is needed to compute the Laplace operator by simple addition of all three entries. The choice of the additional elements o,p,q being "in plane" with the other elements ensures that $\boldsymbol{D}$ is regular for the vast majority of unstructured finite-element meshes. This procedure is not only very fast, but also very accurate, as can be seen from Figs. 5 and 6. For more details, we refer to the original publication [17].

Material nonlinearities

Optimization of material anisotropy

The presented approach to thermodynamic topology optimization is prone to expansion by material nonlinearities: the required additional evolution equations can be derived from the very same principle such that all coupling terms appear automatically. Furthermore, the description of topology optimization by means of evolution equations enables a simultaneous evaluation of the evolution equations that describe the material behavior. Here, we present two examples. We start with the optimization of anisotropic materials, originally published in [19], in which we simultaneously optimize the topology as well as the local material orientation. The second example investigates a tension/compression-sensitive material [11], e.g. reinforced concrete.

A feasible description of an evolving material anisotropy, which may be interpreted as an evolving orientation distribution function, is given by the approach in [20]. The anisotropic stiffness matrix is rotated by means of rotation matrices. In this case, it turns out to be beneficial to use the notation of Mehrabadi-Cowin [32], which is indicated by the subscript $(\cdot)_6$. The Helmholtz free energy is then formulated as

$$\begin{aligned} &\Psi_{\mathrm{m}}^{\mathrm{aniso}} = \\ &\frac{1}{2}\boldsymbol{\sigma}_6\cdot\left[f(\chi)\boldsymbol{Q}_6^T(\boldsymbol{\alpha})\cdot\mathbb{E}_6\cdot\boldsymbol{Q}_6(\boldsymbol{\alpha})\right]^{-1}\cdot\boldsymbol{\sigma}_6 \end{aligned} \tag{40}$$

whereas the energy for regularization Ψ_{r} is taken as in Eq. (24) and $\Psi = \Psi_{\mathrm{m}}^{\mathrm{aniso}} + \Psi_{\mathrm{r}}$. The rotation matrices are parameterized by Euler angles $\boldsymbol{\alpha} = (\varphi(\boldsymbol{x}),\nu(\boldsymbol{x}),\omega(\boldsymbol{x}))$. Other parameterizations are also possible, e.g. Rodrigues parameters or Quaternions, which, however, do not provide additional benefit at increased mathematical/numerical complexity [45].

The dissipation function is chosen as

$$\begin{aligned} \Delta &= \frac{1}{2}\eta\dot{\chi}^2 + \frac{1}{2}r\frac{|\boldsymbol{\sigma}|^2}{1-\cos^2\nu}\left|\dot{\boldsymbol{Q}}\cdot\boldsymbol{Q}^{-1}\right|^2 \\ &= \frac{1}{2}\eta\dot{\chi}^2 + \frac{1}{2}r\frac{|\boldsymbol{\sigma}|^2}{1-\cos^2\nu}\big(\dot{\varphi}^2+\dot{\nu}^2 \\ &\quad + \dot{\omega}^2 + 2\dot{\varphi}\dot{\omega}\,\cos\nu\big) \,, \end{aligned} \tag{41}$$

where $|\dot{\boldsymbol{Q}}\cdot\boldsymbol{Q}^{-1}|^2$ instead of $|\boldsymbol{\alpha}|^2$ ensures objectivity. Inserting Ψ_{m} according to Eq. (40) together with the regularization part Ψ_{r} in Eq. (24) and Δ according to Eq. (41) into the Hamilton principle yields

$$\begin{aligned} &\delta\mathcal{G} + \int_\Omega\left(\frac{\partial\Delta}{\partial\dot{\chi}}\delta\chi + \frac{\partial\Delta}{\partial\dot{\boldsymbol{\alpha}}}\cdot\delta\boldsymbol{\alpha}\right)\,\mathrm{d}V \\ &+\int_\Omega\gamma\delta\chi\,\mathrm{d}V + \lambda\int_\Omega g'(\chi)\delta\chi\,\mathrm{d}V = 0 \\ &\qquad \forall\delta\boldsymbol{u},\ \delta\chi,\ \delta\boldsymbol{\alpha} \,. \end{aligned} \tag{42}$$

Evaluation of the stationarity condi-

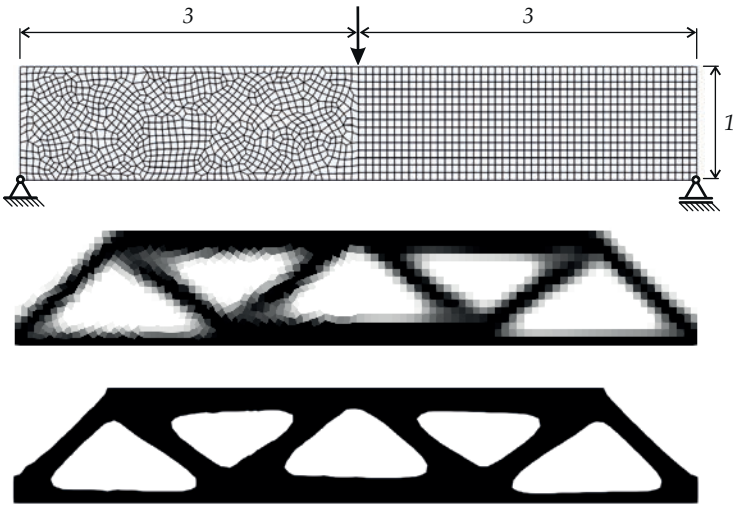

Figure 5: Result for a 2D example using the neighbored-element method for computation of the Laplace operator. The results coincide for the left- and the right-hand sides, even though a structured and an unstructured mesh are used in the very same finite-element simulation. The bottommost picture shows the isosurface representation obtained via graphical post-processing.

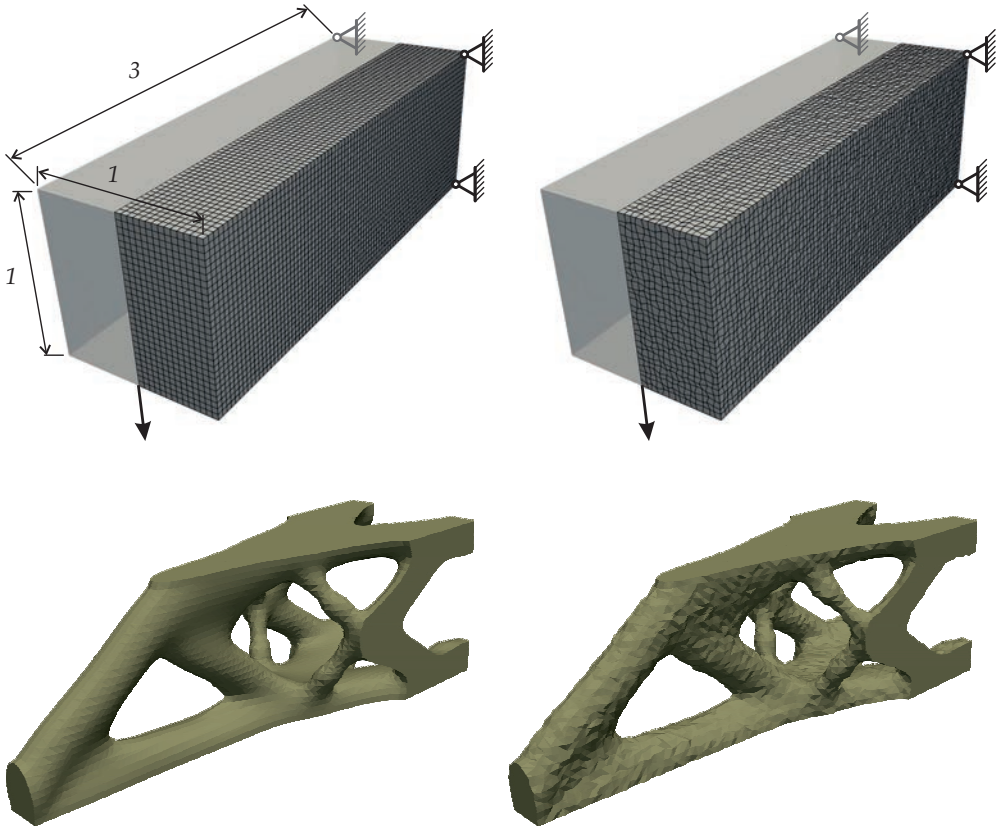

Figure 6: Result for a 3D example using the neighbored-element method for computation of the Laplace operator. Both a structured and an unstructured mesh are used. The isosurface related to the design variable is visualized.

tions gives for the design variable

$$-p_{\mathrm{m}}^{\mathrm{aniso}} + \eta\dot{\chi} + \lambda + \gamma - \beta\nabla^2\chi = 0 \quad \forall x \in \Omega \tag{43}$$

$$\beta\nabla\chi \cdot \boldsymbol{n} = 0 \quad \forall x \in \partial\Omega \ , \tag{44}$$

with $p_{\mathrm{m}}^{\mathrm{aniso}} = -\partial\Psi_{\mathrm{m}}^{\mathrm{aniso}}/\partial\chi$ and for the Euler angles (after a small rearrangement)

$$\dot{\boldsymbol{\alpha}} = \begin{pmatrix} \dot{\varphi} \\ \dot{\nu} \\ \dot{\omega} \end{pmatrix} = \frac{1}{\sqrt{2}r|\boldsymbol{\sigma}|^2} \begin{pmatrix} p_\varphi - p_\omega \cos\nu \\ p_\nu\left(1 - \cos^2\nu\right) \\ p_\omega - p_\varphi \cos\nu \end{pmatrix} \tag{45}$$

with the driving forces for the Euler angles $p_\varphi = -\partial\Psi_{\mathrm{m}}^{\mathrm{aniso}}/\partial\varphi$, $p_\nu = -\partial\Psi_{\mathrm{m}}^{\mathrm{aniso}}/\partial\nu$, and $p_\omega = -\partial\Psi_{\mathrm{m}}^{\mathrm{aniso}}/\partial\omega$. Since the driving forces are derived from the same potential $\Psi_{\mathrm{m}}^{\mathrm{aniso}}$, the evolution of the topology, indicated by χ, and the evolution of the material orientation, parameterized by α, are coupled. For the Laplace operator in Eq. (43), the neighbored-element method as presented in the preceding section is applied. A numerical example is shown in Fig. 7. More details can be found in [19].

Optimization of multi-material systems

A tension/compression enhancement to topology optimization is presented in [11]. To this end, the stress is decomposed into tension $\boldsymbol{\sigma}_+$ and compression $\boldsymbol{\sigma}_-$ parts via

$$\boldsymbol{\sigma}_+ = \sum_{i=1}^{3} \sigma_i \boldsymbol{e}_i \boldsymbol{e}_i \quad \forall\ \sigma_i \geq 0 \ , \qquad \boldsymbol{\sigma}_- = \boldsymbol{\sigma} - \boldsymbol{\sigma}_+ \ , \tag{46}$$

with the principal stresses σ_i, which equal the eigenvalues of $\boldsymbol{\sigma}$. Inserting the stress decomposition into the Helmholtz free energy yields

$$\Psi_0 = \underbrace{\frac{1}{2}\sigma_+ : \mathbb{E}^{-1} : \boldsymbol{\sigma}_+}_{=:\Psi_+} + \underbrace{\frac{1}{2}\sigma_- : \mathbb{E}^{-1} : \boldsymbol{\sigma}_-}_{=:\Psi_-} + \underbrace{\sigma_+ : \mathbb{E}^{-1} : \boldsymbol{\sigma}_-}_{=:\Psi_{+-}} \ . \tag{47}$$

We then define the local measures for local tension- or compression-dominated load states as

$$R_- := \frac{\Psi_-}{\Psi_0} \ , \quad R_+ := \frac{\Psi_+ + \Psi_{+-}}{\Psi_0} \quad \Rightarrow \quad R_- + R_+ = 1 \ . \tag{48}$$

For the Helmholtz free energy used for thermodynamic topology optimization, we employ

$$\Psi_{\mathrm{m}}^{\mathrm{t/c}} = \frac{1}{2}\boldsymbol{\sigma} : [f(\chi)\mathbb{E}(\zeta)]^{-1} : \boldsymbol{\sigma} \tag{49}$$

together with the same approach for the regularizing part of the energy Ψ_{r}, as given in Eq. (24). For the tension/compression enhancement, we introduce the variable $\zeta \in [0,1]$, which is an additional internal variable that indicates the tension-affine material ($\zeta = 0$, e.g. steel) and the compression-affine material ($\zeta = 1$, e.g. concrete). The tension/compression enhancement is an economical goal: the trivial physical answer would be to use the material with higher stiffness, e.g. steel, everywhere. Since steel is more expansive than concrete, steel shall only be used where it is unavoidable, i.e. in tension-dominated regions. We consequently introduce the penalization functional $\mathcal{P}$ as

$$\mathcal{P} = \int_\Omega \left[\zeta R_+ + (1-\zeta)R_-\right] \ \mathrm{d}V \ , \tag{50}$$

which penalizes a tension-affine material for a compression-dominated stress state and vice versa. Accordingly, an appropriate choice for the effective, homogenized elasticity tensor has been made. One possible choice is a Reuss bound in ζ, yielding

$$\mathbb{E}(\zeta) = [\zeta\mathbb{E}_-^{-1} + (1-\zeta)\mathbb{E}_+^{-1}]^{-1} \ . \tag{51}$$

The dissipation function is chosen as

$$\Delta = \Delta_\chi + \Delta_\zeta = \frac{1}{2}\eta\dot{\chi}^2 + \frac{1}{2}\mu\dot{\zeta}^2 \ , \tag{52}$$

with the viscosity μ for the phase variable. For the inclusion of the constraints for ζ, a Kuhn-Tucker parameter is introduced similarly to the constraint for χ in Eq. (14) as

$$\kappa = \begin{cases} \tilde{\kappa} & : \quad \dot{\zeta} > 0 \wedge \zeta = 1 \\ -\tilde{\kappa} & : \quad \dot{\zeta} < 0 \wedge \zeta = 0 \\ 0 & : \quad \text{else} \end{cases} \tag{53}$$

and

$$\mathcal{C}_\zeta := \int_\Omega \kappa\zeta \ \mathrm{d}V \ . \tag{54}$$

The Hamilton principle is then formulated as

$$\delta\mathcal{G} + \int_\Omega \frac{\partial\Delta_\chi}{\partial\dot{\chi}}\delta\chi \ \mathrm{d}V + \delta\mathcal{C}_\chi = 0 \quad \forall\delta\boldsymbol{u},\ \delta\chi \tag{55}$$

$$\delta\mathcal{P} + \int_\Omega \frac{\partial\Delta_\zeta}{\partial\dot{\zeta}}\delta\zeta \ \mathrm{d}V + \delta\mathcal{C}_\zeta = 0 \quad \forall\delta\zeta \tag{56}$$

to decouple the balance of linear momentum from the phase evolution. Again, the motivation is that otherwise the physical but uneconomical solution of a purely stiff material would be realized.

Evaluation of the stationarity conditions again yield for $\delta\boldsymbol{u}$ the balance of linear momentum in its weak form and for $\delta\chi$ and $\delta\zeta$ the evolution equations and boundary condition

$$-p_{\mathrm{m}}^{\mathrm{t/c}} + \eta\dot{\chi} + \lambda + \gamma - \beta\nabla^2\chi = 0 \quad \forall x \in \Omega \tag{57}$$

$$\beta\nabla\chi \cdot \boldsymbol{n} = 0 \quad \forall x \in \partial\Omega \tag{58}$$

$$R_+ - R_- + \mu\dot{\zeta} + \kappa = 0 \ , \tag{59}$$

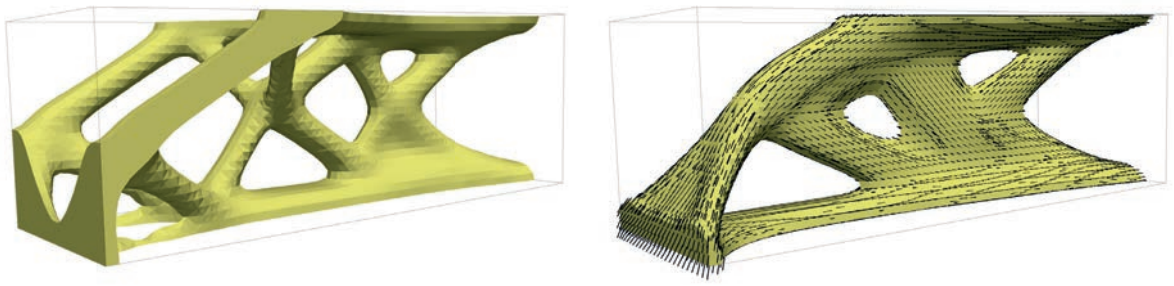

Figure 7: Result for a 3D example of simultaneous thermodynamic topology and material orientation optimization (the boundary value problem is depicted in Fig. 8). Left: result for an isotropic material as a reference solution; right: anisotropic material. The black lines represent the optimal material orientation, e.g. fiber orientation. Obviously, there are significant differences in the optimal structure for the isotropic reference material and the anisotropic material.

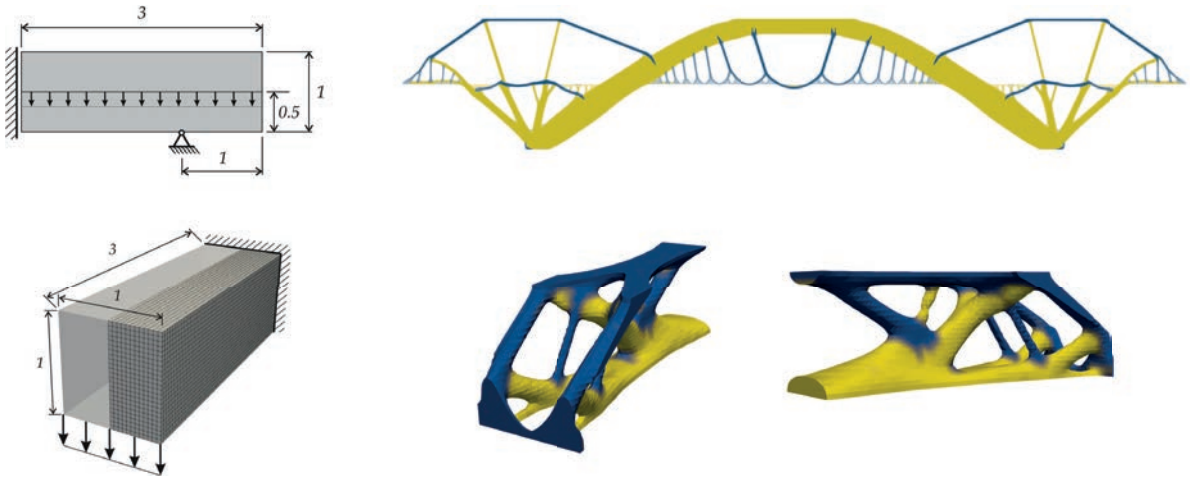

Figure 8: Results for two different boundary value problems using the thermodynamic topology including tension/compression anisotropy. Blue indicates the tension phase (steel) and yellow the compression phase (concrete). Again, there are large deviations as compared to the single-phase material, cf. left-hand side of Fig. 7.

where Eq. (59) can be reformulated to

$$2R_{-} - 1 + \mu\dot{\zeta} + \kappa = 0 \ . \qquad (60)$$

This equation is solved simultaneously to Eq. (57) using an explicit Euler scheme, for which the neighbored-element method is again employed. A numerical example for thermodynamic topology optimization that includes tension/compression anisotropy is presented in Fig. 8.

Conclusions

We showed that thermodynamic extremal principles are also able to yield reasonable results for the problem of topology optimization. To this end, we started with a brief overview of variational principles that are well-known and widely used in material modeling. Motivated by an "inversion of damage models", we used the very same principles to derive the fundamentals of thermodynamic topology optimization. The distribution of mass, which forms the topology of the construction part, is herein described in terms of evolution equations. A nonconvex Helmholtz free energy yields distinct black/white, i.e. solid and void material distributions. As in localization phenomena for damage models, here also numerical issues arise that can be successfully treated by regularization approaches. We presented three different approaches: (i) enhancement by a field function with a penalized gradient and direct penalization of the gradient, which can be numerically treated by (ii) application of a discontinuous Galerkin method or (iii) the neighbored-element method. In the last section, we discussed the inclusion of material nonlinearities into topology optimization. The additional evolution equations can be derived in a straightforward manner from the very same thermodynamic principles as those employed for the mass distribution. Several numerical results highlight the functionality of the thermodynamic topology optimization. Furthermore, the successful application of thermodynamic extremal principles to topology optimization also allows us to reinterpret material models as update schemes for related optimization problems.

References

[1] J Basic, N Degiuli, and D Ban. A class of renormalised meshless laplacians for boundary value problems. *Journal of Computational Physics*, 354:269–287, 2018.

[2] A Bedford. *Hamilton's principle in continuum mechanics*, volume 139. Pitman Advanced Publishing Program, Longman Group, UK, 1985.

[3] MP Bendsøe and O Sigmund. *Topology optimization: theory, methods and applications*. Springer, Berlin, 2003.

[4] V Berdichevsky. *Variational Principles of Continuum Mechanics: I. Fundamentals*. Springer Science & Business Media, Berlin, 2009.

[5] MA Biot. Thermoelasticity and irreversible thermodynamics. *Journal of Applied Physics*, 27(3):240–253, 1956.

[6] D Capecchi and G Ruta. A historical perspective of menabrea's theorem in elasticity. *Meccanica*, 45(2):199–212, 2010.

[7] C Carstensen, K Hackl, and A Mielke. Non–convex potentials and microstructures in finite–strain plasticity. *Proceedings of the Royal Society of London. Series A: Mathematical, Physical and Engineering Sciences*, 458(2018):299–317, 2002.

[8] JD Deaton and RV Grandhi. A survey of structural and multidisciplinary continuum topology optimization: post 2000. *Structural and Multidisciplinary Optimization*, 49(1):1–38, 2014.

[9] B Dimitrijevic and K Hackl. A method for gradient enhancement of continuum damage models. *Technische Mechanik*, 28(1):43–52, 2008.

[10] S Forest and E Lorentz. *Local approach to fracture*, chapter Localization and regularization. Presse des Mines, Paris, 2004.

[11] G Gaganelis, DR Jantos, P Mark, and P Junker. Tension/compression anisotropy enhancement in topology optimization. *under review*.

[12] D Gross and T Seelig. *Fracture mechanics: with an introduction to micromechanics*. Springer, Berlin, 2017.

[13] K Hackl and FD Fischer. On the relation between the principle of maximum dissipation and inelastic evolution given by dissipation potentials. *Proceedings of the Royal Society A: Mathematical, Physical and Engineering Science*, 464(2089):117–132, 2008.

[14] K Hackl, FD Fischer, and J Svoboda. A study on the principle of maximum dissipation for coupled and non-coupled non-isothermal processes in materials. *Proceedings: Mathematical, Physical and Engineering Sciences*, 467(2128):1186–1196, 2011.

[15] WR Hamilton. On a general method in dynamics; by which the study of the motions of all

free systems of attracting or repelling points is reduced to the search and differentiation of one central relation, or characteristic function. *Philosophical transactions of the Royal Society of London*, 124:247–308, 1834.

[16] WR Hamilton. Second essay on a general method in dynamics. *Philosophical Transactions of the Royal Society of London*, 125:95–144, 1835.

[17] DR Jantos, K Hackl, and P Junker. A accurate and fast regularization approach to thermodynamic topology optimization. *International Journal for Numerical Methods in Engineering*, page accepted for publication, 2018.

[18] DR Jantos, P Junker, and K Hackl. An evolutionary topology optimization approach with variationally controlled growth. *Computer Methods in Applied Mechanics and Engineering*, 310:780–801, 2016.

[19] DR Jantos, P Junker, and K Hackl. Optimized growth and reorientation of anisotropic material based on evolution equations. *Computational Mechanics*, 62(1):47–66, 2018.

[20] P Junker. A novel approach to representative orientation distribution functions for modeling and simulation of polycrystalline shape memory alloys. *International Journal for Numerical Methods in Engineering*, 98(11):799–818, 2014.

[21] P Junker and K Hackl. A thermo-mechanically coupled field model for shape memory alloys. *Continuum Mechanics and Thermodynamics*, 26(6):859–877, 2014.

[22] P Junker and K Hackl. A variational growth approach to topology optimization. *Structural and Multidisciplinary Optimization*, 52(2):293–304, 2015.

[23] P Junker and K Hackl. A discontinuous phase field approach to variational growth-based topology optimization. *Structural and Multidisciplinary Optimization*, 54(1):81–94, 2016.

[24] P Junker, S Jaeger, O Kastner, G Eggeler, and K Hackl. Variational prediction of the mechanical behavior of shape memory alloys based on thermal experiments. *Journal of the Mechanics and Physics of Solids*, 80:86–102, 2015.

[25] P Junker, J Makowski, and K Hackl. The principle of the minimum of the dissipation potential for non-isothermal processes. *Continuum Mechanics and Thermodynamics*, 26(3):259–268, 2014.

[26] P Junker, S Schwarz, J Makowski, and K Hackl. A relaxation-based approach to damage modeling. *Continuum Mechanics and Thermodynamics*, 29:291–310, 2017.

[27] A Klarbring and B Torstenfelt. Dynamical systems and topology optimization. *Structural and Multidisciplinary Optimization*, 42(2):179–192, 2010.

[28] A Klarbring and B Torstenfelt. Dynamical systems, simp, bone remodeling and time dependent loads. *Structural and Multidisciplinary Optimization*, 45(3):359–366, 2012.

[29] DM Kochmann and K Hackl. The evolution of laminates in finite crystal plasticity: a variational approach. *Continuum Mechanics and Thermodynamics*, 23(1):63–85, 2011.

[30] E Kuhl, A Menzel, and P Steinmann. Computational modeling of growth. *Computational Mechanics*, 32(1-2):71–88, 2003.

[31] K Langenfeld, P Junker, and J Mosler. Quasi-brittle damage modeling based on incremental energy relaxation combined with a viscous-type regularization. *Continuum Mechanics and Thermodynamics*, 30(5):1125–1144, 2018.

[32] MM Mehrabadi and SC Cowin. Eigentensors of linear anisotropic elastic materials. *The Quarterly Journal of Mechanics and Applied Mathematics*, 43(1):15–41, 1990.

[33] C Miehe, E Gürses, and M Birkle. A computational framework of configurational-force-driven brittle fracture based on incremental energy minimization. *International Journal of Fracture*, 145(4):245–259, 2007.

[34] C Miehe, J Schotte, and M Lambrecht. Homogenization of inelastic solid materials at finite strains based on incremental minimization principles. application to the texture analysis of polycrystals. *Journal of the Mechanics and Physics of Solids*, 50(10):2123–2167, 2002.

[35] A Mielke. Energetic formulation of multiplicative elasto-plasticity using dissipation distances. *Continuum Mechanics and Thermodynamics*, 15(4):351–382, 2003.

[36] A Mielke, F Theil, and VI Levitas. A variational formulation of rate-independent phase

transformations using an extremum principle. *Archive for Rational Mechanics and Analysis*, 162(2):137–177, 2002.

[37] J Mosler and OT Bruhns. On the implementation of rate-independent standard dissipative solids at finite strain–variational constitutive updates. *Computer Methods in Applied Mechanics and Engineering*, 199(9-12):417–429, 2010.

[38] L Onsager. Reciprocal relations in irreversible processes. i. *Physical Review*, 37(4):405–426, 1931.

[39] L Onsager. Reciprocal relations in irreversible processes. ii. *Physical Review*, 38(12):2265, 1931.

[40] M Ortiz and L Stainier. The variational formulation of viscoplastic constitutive updates. *Computer Methods in Applied Mechanics and Engineering*, 171(3):419–444, 1999.

[41] C Prax, H Sadat, and P Salagnac. Diffuse approximation method for solving natural convection in porous media. *Transport in Porous Media*, 22(2):215–223, 1996.

[42] H Pulte. *Das Prinzip der Kleinsten Wirkung und die Kraftkonzeptionen der Rationalen Mechanik – Eine Untersuchung zur Grundlegungsproblematik bei Leonhard Euler, Pierre Louis Moreau de Maupertuis und Joseph Louis Lagrange*. Franz Steiner Verlag, Stuttgart, 1989.

[43] GIN Rozvany. A critical review of established methods of structural topology optimization. *Structural and Multidisciplinary Optimization*, 37(3):217–237, 2009.

[44] O Sigmund and J Petersson. Numerical instabilities in topology optimization: a survey on procedures dealing with checkerboards, mesh-dependencies and local minima. *Structural Optimization*, 16(1):68–75, 1998.

[45] J Stuelpnagel. On the parametrization of the three-dimensional rotation group. *SIAM Review*, 6(4):422–430, 1964.

[46] T Waffenschmidt and A Menzel. Application of an anisotropic growth and remodelling formulation to computational structural design. *Mechanics Research Communications*, 42:77–86, 2012.

[47] M Zhou, YK Shyy, and HL Thomas. Checkerboard and minimum member size control in topology optimization. *Structural and Multidisciplinary Optimization*, 21(2):152–158, 2001.

Topology optimization beyond linear elasticity

by Mathias Wallin[1] and Daniel Tortorelli[2]

[1]Division of Solid Mechanics, Lund University, Sweden
[2]Center for Design and Optimization, Lawrence Livermore National Laboratory, CA, USA

Abstract

Complex, non-linear path-dependent and transient response of engineering structures can today be numerically modeled with good accuracy. For linear systems, this modeling has successfully been combined with computational design optimization for many years. The combination of non-linear modeling and numerical design optimization is far less established. In the present paper we discuss some recent steps taken to close the gap between the use of linear and non-linear modeling with numerical optimization. Examples with nonlinear elasticity, finite strain plasticity and dynamic modeling combined with topology optimization are discussed.

Introduction

Since the work by Bendsøe and Kikuchi (1989) there has been a tremendous development of numerical methods tailored for the optimal topology design of materials and structures. Topology optimization has been applied problems at the structural scale to design bridges as well as the microscale to design composite microstructures with exotic effective properties such negative Poissons ratio and negative thermal expansion. The method has primarily been applied to elastic structural problems but it has also been used to design structures for optimal for thermal, fluid and wave propagation responses. Non-gradient based optimization algorithms exist to solve these problems, however they are not practical due to their large computational cost. As such nonlinear programming algorithms that rely on gradient information are dominating. That said, the number of design variables in topology optimization is very large so the direct computation of the gradients, by e.g. the forward differences, is also prohibitively costly. To overcome this hurdle, the adjoint approach for calculating the gradients, i.e. the sensitivities, is generally employed. The adjoint approach requires the solution of an adjoint field for each objective and constraint function in addition to the primal response, e.g. the displacement field. However the adjoint responses are governed by linear systems as opposed to the primal response that is governed by nonlinear systems. Once the adjoint responses are obtained, the sensitivities of the cost and constraint functions are obtained with respect to any number of design variables with an insignificant amount of computation.

Because the optimization problem is nonlinear, gradient-based nonlinear programming algorithms solve them iteratively. In each iteration the design is evaluated by solving the state problem, i.e. the equations of motion or equilibrium equations for quasi-static conditions and evaluating the objective and constraints functions. Next the adjoint problems are solved and the sensitivities of the objective and constraint functions with respect to the design variables are evaluated. Based on the gradient information, a convex approximation of the design space is established via e.g the Method of Moving Asymptotes (MMA) (Svanberg 1987). Since the MMA approximation is both convex and separable, the approximative subproblem can be efficiently solved for the next design iteration using a dual formulation. Iterations are repeated until the design changes between successive iterations are small. Even though the subproblem is convex, optimization problems are rarely convex and consequently multiple local minima are expected. The engineering approach to reduce the influence of multiple local minima is to run the problem for a number of initial conditions and thereby increase the likelihood of finding the global optimum.

For structures operating in the linear regime, the numerical design optimization procedure described above has successfully been used to generate optimal designs. Simple optimization objectives related to stiffness and eigen-frequency for linear elastic structures can be accommodated with commercial software packages that are used on daily basis in industry. Numerical models that can predict the non-linear and irreversible response of structures are also well established, however the link that connects these models to optimization schemes is lacking.

Topology optimization problem

Topology optimization is aimed towards finding the optimal layout of material within a given design domain that minimizes (or maximizes) the objective function and satisfies given constraints. The structure is discretized using finite elements and

each element in the design domain is assigned a binary valued scalar design variable z_i which defines if the element is filled $z_i = 1$ or void $z_i = 0$. To enable gradient based methods, the problem is regularized such that the binary valued design variables are replaced by real valued variables that take on z_i value in the interval [0 1], where again the element is filled if $z_i = 1$ or void if $z_i = 0$, otherwise it is partially filled. To model the material stiffness of partially filled elements and to limit the regions with partially filled elements, i.e. gray regions, the Solid Isotropic Material with Penalization (SIMP) scheme (Bendsøe (1989)) is frequently employed, i.e.,

$$E_i = z_i^p \, E_0$$

where E_i and E_0 represent the Youngs modulus for the partially filled and full elements, respectively. The exponent p typically is chosen as 3 and it is introduced to penalize the gray interface regions. A common alternative to the SIMP interpolation is the RAMP (Stolpe and Svanberg (2001)) scheme which we opt to use. It is well-known that this regularized/penalized approach results in an ill-posed optimization problem that is characterized by mesh dependent and checker-board designs. To generate a well-posed problem a minimum length scale on the design field chatter is imposed, e.g. by filtering the design variables using e.g. via a convolution filter (Bruns and Tortorelli (2001)) or a PDE filter cf. Lazarov and Sigmund (2011). The density based filter approach can be summarized in that the design variable z_i for the stiffness computation is replaced by the filtered variable ρ_i defined as

$$\rho_i = \int_{B_r(z_i)} w(x_i - y)\, z(y)\, \mathrm{d}v$$

where $B_r(x_i)$ is the area over which we average, w the kernel function and x_i is the centroid of element i.

Application examples

To demonstrate the possibility to include complex non-linear response in topology optimization, a number of examples are shown below. For linear systems, the optimal design is independent of the load path. When structures are optimized under nonlinear elastic response, the optimal design depends on the load level. Likewise, for transient and elastoplastic response the optimal design depends not only on the final load level, but also on the load trajectory.

Most of the computational time spent in a design update is due to the solution of the state problem. For transient and path-dependent problems, the state problem needs to be solved over the entire load history. For nonlinear elastic systems, the state from the previous design can be used as a predictor for the current simulation to hasten the solution process. The cost for the sensitivity analysis can also be significant for transient and path-dependent problems since the stiffness matrices from all time steps are required for the sensitivity analysis. For small and moderate size problems, the stiffness matrices required in the sensitivity analysis can be stored and reused, otherwise they need to be recalculated.

Stiffness optimization of non-linear structures

A common objective of small strain and linear elastic topology optimization is structural stiffness maximization subject to a constraint on the structural mass. For linear elastic systems this objective can be defined via the scalar product of the applied load and the discretized displacement field. This objective has the advantage that the adjoint and primal states are equal which simplifies the sensitivity computations. The generalization of linear elastic stiffness objective function to nonlinear systems is not unique. Obviously the definition of stiffness plays an important role for the optimized design. To illustrate the difference between possible stiffness definitions, consider Fig. 1 where the response of a non-linear structure is depicted by the solid line. The commonly used secant stiffness (dashed line) is, for a fixed load level, equivalent to displacement minimization. Alternatively, the tangent stiffness (dotted line) indicates the incremental stiffness about the current load level to a differential load increment; it is used to determine a structures susceptibility to buckling and bifurcation. From this observation we note that a structure that is deemed stiff via a large secant stiffness might, in fact, be at the risk of immediate collapse due to a zero tangent stiffness. For this reason we optimize the tangent stiffness objective.

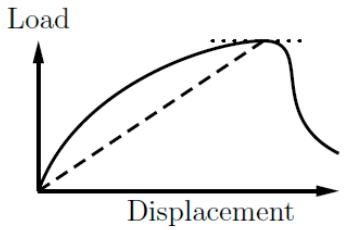

Figure 1: Illustration of secant and end-tangent stiffness definitions.

The available research on finite strain topology optimization is primarily based on Saint-Venants elastic material model, i.e. a linear relation between second Piola stress and the Green-Lagrange strain is assumed. This model is adequate for large displacement and small strain situations, however it performs poorly if large strain is encountered, we therefore use a neo-Hookean material model. This choice increases the complexity of the sensitivity analysis,

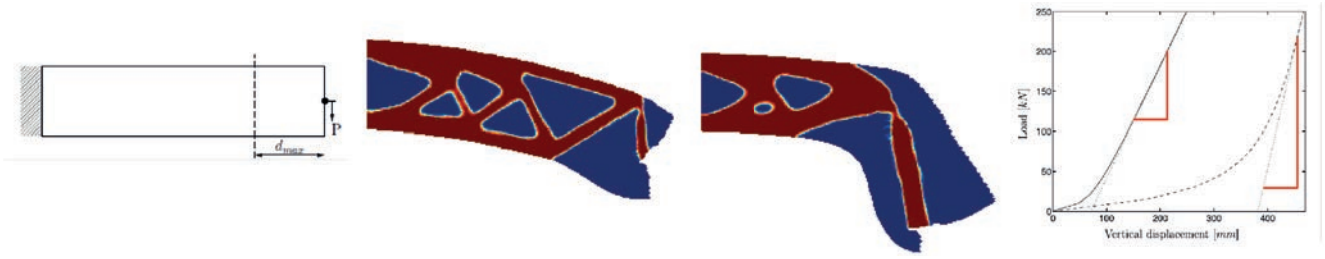

Figure 2: Optimal design of a cantilever beam using secant and end-tangent stiffness definitions.

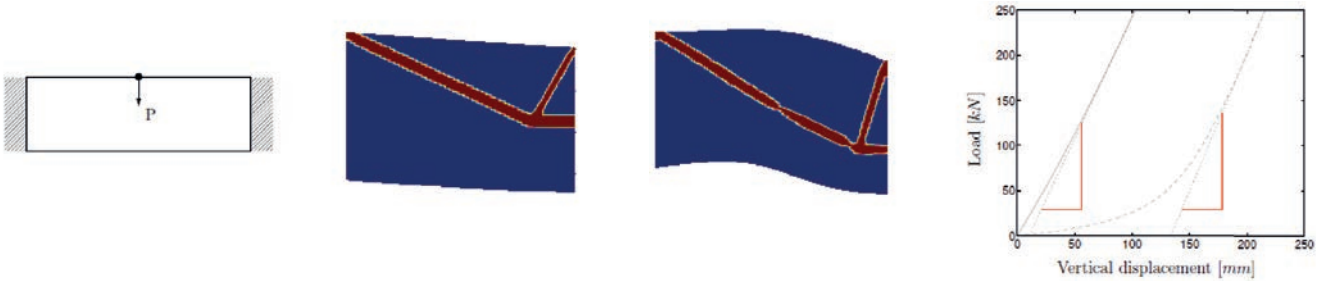

Figure 3: Optimal design of a double clamped beam using secant and end-tangent stiffness definitions.

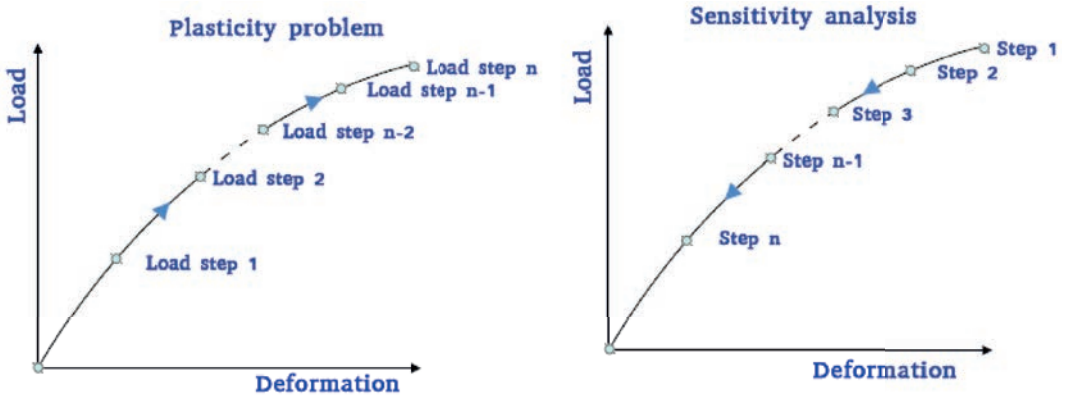

Figure 4: Illustration of the reversed procedure used to calculate the sensitivity for path-dependent problems.

however, as shown in Wallin et al. (2018) standard finite element routines can be used to form the sensitivity.

Topology optimization creates void, or nearly void regions in the structure and this leads to convergence problems of the primal analysis as the elements in these undergo large deformation which cause the finite elements to invert. One remedy to this problem is to remove and reintroduce elements in these regions as proposed by Bruns and Tortorelli (2003). An alternative uses a transition function such that the void regions are modeled by linear elasticity and the solid regions by the intended nonlinear material models, cf. Wang et al. (2014). The latter approach is used herein.

Kemmler et al. (2005) investigated different stiffness objectives in conjunction with stability. Their formulation was restricted to moderate strain due to their use of the Saint-Venant material model. To show the influence of large deformations we present designs were we consider the secant and tangent stiffness objectives, cf. Wallin et al. (2018). We use well-known structures to illustrate the design differences. First, the cantilever beam shown in Fig. 2a is optimized using the secant and the end-tangent stiffness definitions.

Fig. 2b, shows the secant stiffness design. In contrast to structures optimized for linear elasticity, we observe that the optimal design adapts to the applied load and that the void regions are highly distorted. For the tangent stiffness objective the beam would rotate 90 degrees clockwise to align with the load direction and thereby creating a pure tensile state. The extremely large deformations experienced by this design prevents us from simulating the state problem. So to illustrate the effect of the tangent stiffness objective, we introduce a constraint on the motion of the point (P) where the load is applied. The constraint is formulated such that the point (P) is restricted to not move left of the dashed line which is located 30% of the beam length from the beams right end. Using the tangent stiffness objective together with this constraint renders a structure with a hinge-like topology, i.e. a short beam with an appended bar, cf. Fig. 2c. In Fig. 2d the responses of the designs in Fig. 2b and Fig. 2c are shown where it is seen that the tangent stiffness is higher for the design in Fig. 2c whereas the tip deflection is less for the design in Fig. 2b.

In a second example a double clamped beam subjected to the top center vertical point load P is optimized using the secant and tangent stiffness objectives. We impose design symmetry with respect to reflections about the center vertical axis so there is no need to limit the horizontal displacement of the load point. If this symmetry is not enforced the tangent objective will produce a design that detaches from one of the supports to generate a tensile state as discussed in the cantilever beam example. Again, two very different designs are obtained. The structure optimized for secant stiffness (Fig. 3b) is less deformed compared to the structure optimized for tangent stiffness (Fig. 3c). As expected the design optimized for tangent stiffness shows a steeper terminal slope as shown in Fig. 3d whereas the design optimized for secant stiffness deforms less. From these examples we conclude that the generalization of linear elastic stiffness optimization to the nonlinear regime is not trivial because the choice of objective greatly influences the optimized design.

Optimal design of energy absorbing structures

Path-dependent material response in combination with topology optimization is rare and the research that addresses this response has thus been limited to small strains, cf. e.g. Maute et al. (1998) and Pedersen (2004). Small strain formulations are of lesser relevance for energy mitigating structural and material designs as they are intended to experience large strains. Additionally, the energy mitigation occurs at elevated strain rates, and hence viscoplasticity and inertial must be considered in their design.

The path-dependence of plastically deforming materials requires the load history to be considered during both the primal and adjoint solutions. In secant stiffness based optimization one adjoint problem needs to be solved in addition to the primal problem, whereas two adjoint problems must be solved in the tangent stiffness based optimization. For the path-dependent problems the sensitivity analysis is much more challenging since adjoint fields for each time step are required as well as adjoint variables associated with the constitutive laws in each integration point are needed. For transient problems, adjoints for the velocity and acceleration fields are also introduced. The adjoint approach for the transient visco-plastic problem becomes a terminal value problem, i.e. first the primal visco-plastic problem is solved and then based on the primal solution we calculate the sensitivity, cf. Fig. 4. A general description of adjoint sensitivity of transient elasto-plastic problems can be found in Michaleris et al. (1994).

Recently, we extended the topology optimization framework to accommodate designs which experience

Figure 5: Double clamped beam optimimzed for maximum energy absorbation using rate-independent plasticity under quasi static conditions.

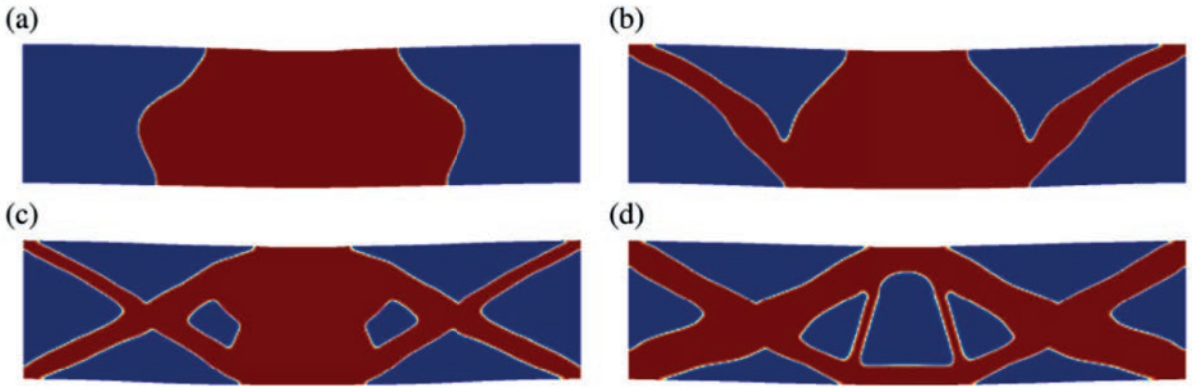

Figure 6: Double clamped beam optimimzed for maximum visco-plastic energy absorbation. The designs are obtained for a) high loading rate to d) nearly quasi-static loading rates.

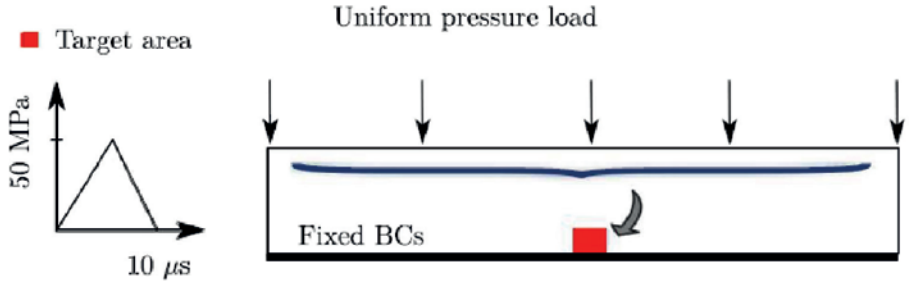

Figure 7: Boundary conditions for a plate optimized to guide an incoming wave into a target area

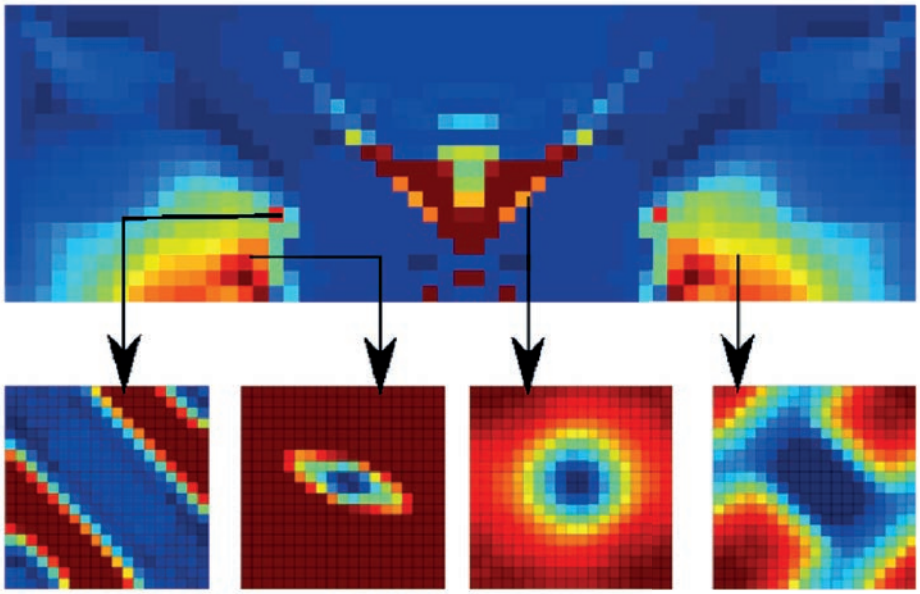

Figure 8: Macro and micro optimized design for guidance of an incoming pressure wave to a target area.

large elastic and plastic strains, cf. Wallin et al. (2016). The primal solution for the elasto-plastic response is obtained by using conventional numerical procedures, i.e. finite element discretization in space, backward-Euler time integration of the constitutive laws and Newton-Raphson iterations. The template constitutive model that we considered is an isothermal, isotropic hardening plasticity model, cf. Simo and Miehe (1992).

In Fig. 5a double clamped beam is optimized for maximum plastic energy absorption defined as

$$W^p = \int_0^T \int_V \dot{w}^p \, \mathrm{d}v \, \mathrm{d}t$$

where $\dot{w}^p$ is the rate of the specific plastic work, T is the terminal time and V is volume of design domain. A constraint on the structural volume is also imposed. In Fig. 5b the symmetric part of the optimal material layout is shown in the deformed configuration whereas the specific plastic work appears in Fig. 5c.

Since energy mitigation is associated with high impact velocities, we also consider dynamic visco-plastic response for the design of energy mitigating structures, cf. Ivarsson et al. (2018). The simple double clamped beam shown in Fig. 5a is again designed to maximize visco-plastic work subject to a mass constraint. But here we consider load rates ranging from slow (quasi-static) to very fast. For the highest load rates the optimal design is not attached to the supporting wall as no forces will be transferred to the supports over the small load duration. As the load rate decreases more and more connections to the supporting wall is made. The design obtained for the lowest, nearly quasi-static, load rate coincides with the quasi static elasto-plastic results presented in Wallin et al. (2016).

Nonlinear dynamic topology optimization is not restricted to design of macro-structures. In Nakshatrala and Tortorelli (2016), a multi-scale optimization scheme was used to design nonlinear elastic energy mitigating structures. At the microlevel, the material is modeled as nonlinear neo Hookean while the macroscopic material response is obtained from homogenization of the microstructural response. The procedure is applied to the boundary value problem in shown in Fig. 7. The plate is subjected to a uniform triangular pulse at the upper part of the boundary as shown in Fig. 7.

The goal of the optimization is to maximize the total potential plus kinetic energy to the target red square at the plates bottom center region. Fig. 8 illustrates the optimized macro and some of the microstructural designs. The colors indicate the macro and micro scale volume fraction ranging from pure stiff red material to pure compliant blue material. Not surprisingly the optimal microstructure is highly heterogeneous and hence the optimal design is impossible to predict based on engineering intuition alone.

Conclusions

The vast majority of the research and applications of topology optimization

assume linear elastic response. In this paper we have, through several examples, showed that it is possible to incorporate complex material response and dynamics in conventional topology optimization. The generalization to nonlinear dynamic response requires more thought about the objective functions and loadings, and in particular the loading rate.

Acknowledgement

This work was performed under the auspices of the U.S. Department of Energy by Lawrence Livermore Laboratory under Contract DE-AC52-07NA27344. The financial support from the Swedish research council (grant ngb. 2015-05134), Åforsk and Crafoord foundation (grant ngb. 20180527) are also gratefully acknowledged.

References

Bendsøe, M. P., & Kikuchi, N. (1988). Generating optimal topologies in structural design using a homogenization method. Computer Methods in Applied Mechanics and Engineering, 71(2), 197–224.

Bendsøe, M. P. (1989). Optimal shape design as a material distribution problem. Structural Optimization, 1(4), 193–202.

Bruns, T. E., & Tortorelli, D. A. (2001). Topology optimization of non-linear elastic structures and compliant mechanisms. Computer Methods in Applied Mechanics and Engineering, 190(26-27), 3443–3459.

Bruns, T. E., & Tortorelli, D. A. (2003). An element removal and reintroduction strategy for the topology optimization of structures and compliant mechanisms. International Journal for Numerical Methods in Engineering, 57(10), 1413–1430.

Ivarsson, N., Wallin, M., & Tortorelli, D. (2018). Topology optimization of finite strain viscoplastic systems under transient loads. International Journal for Numerical Methods in Engineering, 114(13), 1351–1367.

Kemmler, R., Lipka, A., & Ramm, E. (2005). Large deformations and stability in topology optimization. Structural and Multidisciplinary Optimization, 30(6), 459–476.

Lazarov, B. S., & Sigmund, O. (2011). Filters in topology optimization based on Helmholtztype differential equations. International Journal for Numerical Methods in Engineering, 86(6), 765–781.

Maute, K., Schwarz, S., & Ramm, E. (1998). Adaptive topology optimization of elastoplastic structures. Structural Optimization, 15(2), 81–91.

Michaleris, P., Tortorelli, D. A., & Vidal, C. A. (1994). Tangent operators and design sensitivity formulations for transient nonlinear coupled problems with applications to elastoplasticity. International Journal for Numerical Methods in Engineering, 37(14), 2471–2499.

Nakshatrala, P. B., & Tortorelli, D. A. (2016). Nonlinear structural design using multiscale topology optimization. Part II: Transient formulation. Computer Methods in Applied Mechanics and Engineering, 304, 605–618.

Pedersen, C. B. (2004). Crashworthiness design of transient frame structures using topology optimization. Computer Methods in Applied Mechanics and Engineering, 193(6-8), 653–678.

Simo, J. C., & Miehe, C. (1992). Associative coupled thermoplasticity at finite strains: Formulation, numerical analysis and implementation. Computer Methods in Applied Mechanics and Engineering, 98(1), 41–104.

Stolpe, M., & Svanberg, K. (2001). An alternative interpolation scheme for minimum compliance topology optimization. Structural and Multidisciplinary Optimization, 22(2), 116–124.

Svanberg, K. (1987). The method of moving asymptotesa new method for structural optimization. International Journal for Numerical Methods in Engineering, 24(2), 359–373.

Wallin, M., Jönsson, V., & Wingren, E. (2016). Topology optimization based on finite strain plasticity. Structural and Multidisciplinary Optimization, 54(4), 783–793.

Wallin, M., Ivarsson, N., & Tortorelli, D. (2018). Stiffness optimization of non-linear elastic structures. Computer Methods in Applied Mechanics and Engineering, 330, 292–307.

Wang, F., Lazarov, B. S., Sigmund, O., & Jensen, J. S. (2014). Interpolation scheme for fictitious domain techniques and topology optimization of finite strain elastic problems. Computer Methods in Applied Mechanics and Engineering, 276, 453–472.

Wang, F., Sigmund, O., & Jensen, J. S. (2014). Design of materials with prescribed nonlinear properties. Journal of the Mechanics and Physics of Solids, 69, 156–174.

Variational design sensitivity analysis and multiscale optimisation

by Franz-Joseph Barthold[1] and Wojciech Kijanski[1]

[1]Chair of Structural Mechanics, Department of Architecture and Civil Engineering, TU Dortmund, Germany

Summary

Nowadays, many structures and mechanical components with practical relevance are built from so-called *high performance materials*. These materials are often classified as homogeneous on the component level (macroscale) but they consist of diverse heterogeneities on the material level (microscale). The modelling and analysis of such complex structures is practised for example in material science, automotive and aerospace industries. Especially methods for numerical homogenisation and so-called FE^2 techniques are suitable for investigations of the physical behaviour on different length scales. Consequently, multiscale analysis (MSA) can be enhanced by methods for multiscale structural optimisation (MSO) to automatically determine improved macro- and microscale layouts.

Keywords

Structural optimisation, sensitivity analysis, numerical homogenisation, FE^2 method, multiscale optimisation, material design

Introduction

Throughout this paper, we assume that the reader is familiar with the central concepts of continuum mechanics and the finite element method on the one hand and the notation of structural optimisation and nonlinear programming on the other hand.

Computational efficient structural optimisation for nonlinear mechanical problems is demanding. To achieve this goal, numerous research areas are involved.

For example, improved modelling of optimisation problems and sophisticated nonlinear programming algorithms are discussed in literature, to name a few. The availability of all gradients of objective and constraint functions with respect to all design parameters characterises the last-mentioned methods.

Roughly, four different approaches to *design sensitivity analysis* can be identified, which are linked to the steps of the development process.

- Continuous variations are derived for sufficiently smooth functions.
- Analytical derivatives are obtained for discrete quantities.
- Automatic differentiation generates code for the derivatives.
- Numerical differentiation is based on the executable software.

All approaches lead to the same numerical value (up to a manageable small perturbation) of the gradients desired by the chosen nonlinear programming method. But the computational efficiency as well as the amount of insight differ significantly between these approaches.

Our research is focused on theory and computation of *variational design sensitivity analysis* (VDSA) and the interpretation of obtained sensitivities. Lewin's saying *There is nothing so practical as a good theory* [9] characterises our approach. The investment into theory pays off and efficient computer algorithms are developed for structural optimisation.

Refined continuum mechanics

The authors' viewpoint on variational design sensitivity analysis within a general continuum mechanical framework relies on a rigorous separation of physical quantities (from the very beginning of the theory) into *design* and *motion* mappings based on intrinsic coordinates, cf. [2, 3, 4]. Thus, continuum mechanics is understood as a theory of two fundamental and independent geometry and motion mappings depicted in Fig. 1. In this presentation, the terms *design* and *geometry* are used synonymously.

In detail, the reference placement $\mathcal{K}$ of the material body with reference points $\mathbf{X} = \boldsymbol{\kappa}_\Theta(\boldsymbol{\Theta}, s)$ is parametrised by intrinsic coordinates $\boldsymbol{\Theta}$ and design s. Similarly, the current placement $\mathcal{M}$ with current points $\mathbf{x} = \boldsymbol{\mu}_\Theta(\boldsymbol{\Theta}, t)$ is parametrised by intrinsic coordinates $\boldsymbol{\Theta}$ and time t. The deformation $\boldsymbol{\varphi}_X$ split into the mappings $\boldsymbol{\varphi}_X = \boldsymbol{\mu}_\Theta \circ \boldsymbol{\kappa}_\Theta^{-1}$, see Fig. 1a. The displacement map $\boldsymbol{\upsilon}_\Theta = \boldsymbol{\mu}_\Theta - \boldsymbol{\kappa}_\Theta$ with $\mathbf{u} = \mathbf{x} - \mathbf{X}$ can be used alternatively.

The intrinsic *motion gradient* $\mathbf{M}_\Theta$ and the intrinsic *geometry gradient* $\mathbf{K}_\Theta$ are used to decompose the referential *deformation gradient* $\mathbf{F}_X = \mathbf{M}_\Theta \mathbf{K}_\Theta^{-1}$, see the tangent mappings in Fig. 1b.

Thus, the cause and the effect of design perturbations can be described in continuum mechanics via variations of either $\boldsymbol{\kappa}_\Theta, \boldsymbol{\mu}_\Theta$ or $\boldsymbol{\kappa}_\Theta, \boldsymbol{\upsilon}_\Theta$. This approach differs conceptually from the material derivative approach [1] and the domain parametrisation approach [16], respectively. The relationship to configurational mechanics is explained in [10, 11].

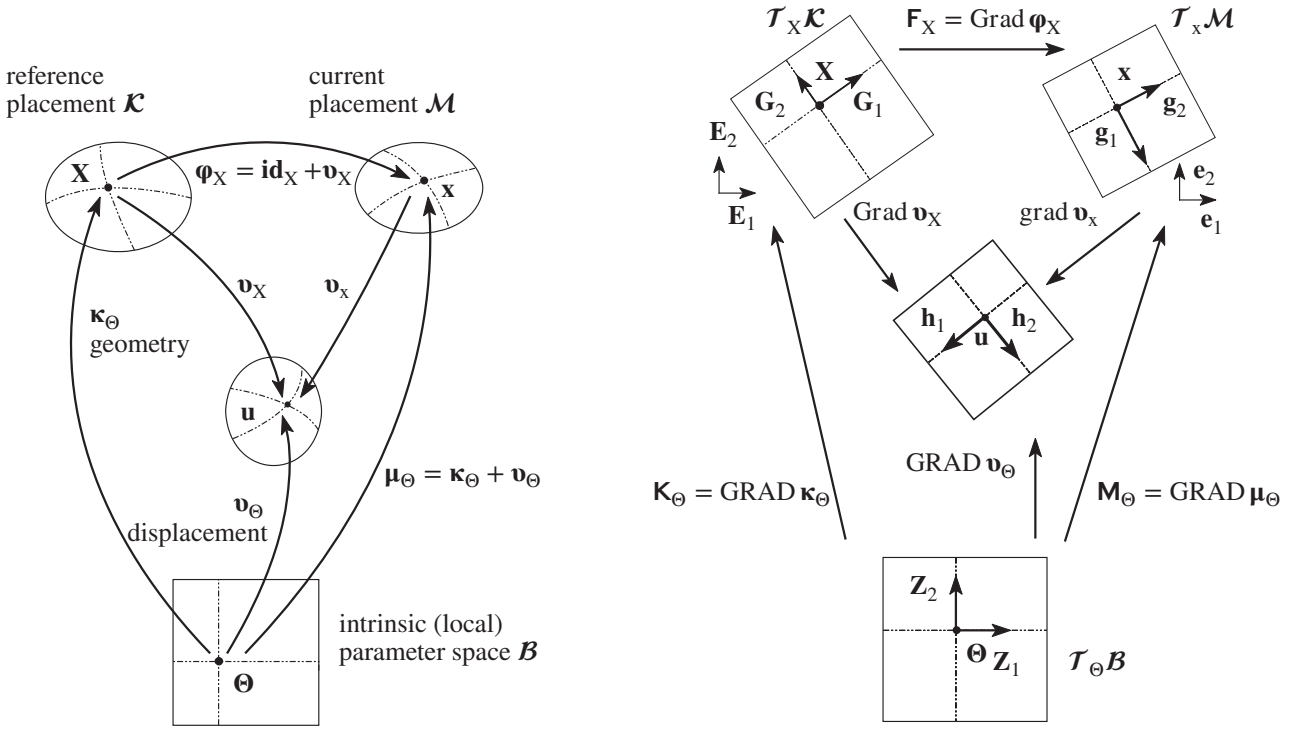

(a) Point mappings between placements.

(b) Tangent mappings between tangent spaces.

Figure 1: Continuum mechanics based on independent geometry and displacement maps.

Variational design sensitivity analysis

Sensitivity analysis of nonlinear mechanical problems is usually organised as staggered scheme. Initially, both mappings ($\boldsymbol{\kappa}_\Theta$ and $\boldsymbol{\upsilon}_\Theta$) defined on the material body using intrinsic coordinates are considered to be independent. In the first step, the weak form

$$R(\mathbf{X}, \mathbf{u}) = 0 \tag{1}$$

implicitly defines the displacement $\mathbf{u}$ for given geometry (design) $\mathbf{X}$. In the second step, perturbations of design are considered. Importantly, these geometry variations $\delta\mathbf{X}$ should generate displacement variations $\delta\mathbf{u}$ such that equilibrium $R = 0$ is not destroyed, i.e.

$$\delta R = \delta_X R + \delta_u R = 0. \tag{2}$$

Its interpretation is the balance of perturbation forces which represent variations of geometry (design) and displacement.

Further analysis leads to the *physical stiffness operator* $k(\mathbf{X}, \mathbf{u}; \boldsymbol{\eta}, \delta\mathbf{u})$ and the *pseudo load operator* $p(\mathbf{X}, \mathbf{u}; \boldsymbol{\eta}, \delta\mathbf{X})$ depending on current geometry $\mathbf{X}$, current displacement $\mathbf{u}$, test function $\boldsymbol{\eta}$, as well as variations $\delta\mathbf{X}$ and $\delta\mathbf{u}$, respectively. Finally, Eq. (2) reads

$$\delta R = p(\delta\mathbf{X}) + k(\delta\mathbf{u}) = 0 \tag{3}$$

and implicitely defines the continuous *sensitivity operator* s

$$\delta\mathbf{u} = s(\delta\mathbf{X}). \tag{4}$$

This relationship is central for the *variational design sensitivity analysis*.

Similarly, the sensitivity of objective or constraint functions $f(\mathbf{X}, \mathbf{u})$ can be formulated. Therefore, $\beta(\mathbf{X}, \mathbf{u}; \delta\mathbf{X})$ and $\gamma(\mathbf{X}, \mathbf{u}; \delta\mathbf{u})$ denote linear forms obtained by varying f with respect to geometry (design) $\mathbf{X}$ or displacements $\mathbf{u}$.

The total variation of f reads

$$\begin{aligned} \delta f &= \delta_X f + \delta_u f \\ &= \beta(\delta\mathbf{X}) + \gamma(\delta\mathbf{u}) \\ &= (\beta + \gamma \circ s)(\delta\mathbf{X}). \end{aligned} \tag{5}$$

Herein, the linear operator a defined as

$$\alpha = \beta + \gamma \circ s \tag{6}$$

represents the complete influence of the design variations on the objective or constraint functions f. Finally, the total variation of f yields

$$\delta f = \alpha(\delta\mathbf{X}). \tag{7}$$

In summary, all necessary information are already available on the continuous level. Unfortunately, some information are only implicitely available and only a few additional theoretical steps are possible. Thus, additional explanations and the computable schemes are given based on the discrete counterparts.

Associated discretisation

All continuous quantities must be discretised to generate a computational scheme. Here, the discretisation of the geometry map $\boldsymbol{\kappa}_\Theta$ follows exactly the same rules as known from the discretisation of structural response, i.e. the displacement map $\boldsymbol{\upsilon}_\Theta$. The presentation is based on intrinsic coordinates in our theory. To exemplify the resulting discrete quantities in a known framework, we summarise the matrices for the standard isoparametric finite element method.

The discrete version of Eq. (2) reads $\delta R = \boldsymbol{V}^{\mathrm{T}}\, \delta \boldsymbol{R} = 0$ with

$$\delta \boldsymbol{R} = \boldsymbol{P}\, \delta \boldsymbol{X} + \boldsymbol{K}\, \delta \boldsymbol{U} = \boldsymbol{0}, \qquad (8)$$

where $\boldsymbol{X}$ are the nodal coordinates and $\boldsymbol{U}$ are the nodal displacements. Thus, the abovementioned bilinear forms k and p generate the *stiffness matrix* $\boldsymbol{K}$ and the *pseudo load matrix* $\boldsymbol{P}$. Importantly, the discretisation of Eq. (4) yields the computable *sensitivity matrix* $\boldsymbol{S}$, which maps any design variation $\delta \boldsymbol{X}$ to the related displacement variation

$$\delta \boldsymbol{U} = -\boldsymbol{K}^{-1}\, \boldsymbol{P}\, \delta \boldsymbol{X} = \boldsymbol{S}\, \delta \boldsymbol{X}. \qquad (9)$$

The wording *pseudo load* can be argued based on the discrete equations. In case of linear problems, $\boldsymbol{R} = \boldsymbol{K}\,\boldsymbol{U} - \boldsymbol{F} = \boldsymbol{0}$ yields $\boldsymbol{U} = \boldsymbol{K}^{-1}\,\boldsymbol{F}$. Similarly, Eq. (9) can be rewritten as $\delta \boldsymbol{U} = \boldsymbol{K}^{-1}\,\boldsymbol{Q}$ with the *pseudo load vector* $\boldsymbol{Q} = -\boldsymbol{P}\,\delta \boldsymbol{X}$. Thus, the pseudo load matrix $\boldsymbol{P}$ transforms a given design perturbation $\delta \boldsymbol{X}$ into a corresponding force vector $\boldsymbol{Q}$. Importantly, both $\delta \boldsymbol{X}$ and $\boldsymbol{Q}$ have the same effect on the perturbation $\delta \boldsymbol{U}$ of the structural response.

Last but not least, the discrete sensitivity equation for objective and constraint functions $f(\boldsymbol{X}, \boldsymbol{U})$ reads

$$\delta f = \boldsymbol{b}^{\mathrm{T}}\, \delta \boldsymbol{X} + \boldsymbol{c}^{\mathrm{T}}\, \delta \boldsymbol{U}, \qquad (10)$$

where $\boldsymbol{b}, \boldsymbol{c}$ denote discrete variations of f with respect to geometry $\boldsymbol{X}$ and displacements $\boldsymbol{U}$, respectively. The combination of Eqs. (10) and (9) yields the discrete counterparts of Eq. (5)

$$\boldsymbol{a}^T = \boldsymbol{b}^{\mathrm{T}} - \boldsymbol{c}^{\mathrm{T}}\, \boldsymbol{K}^{-1}\, \boldsymbol{P} \qquad (11)$$

and finally of Eq. (7)

$$\delta f = \boldsymbol{a}^{\mathrm{T}}\, \delta \boldsymbol{X}. \qquad (12)$$

The central sensitivity information $\boldsymbol{a}$ for any objective or constraint function f can be computed independently from the specific choice of design variation $\delta \boldsymbol{X}$.

Therefore, the geometrical and physical contributions to sensitivity analysis can be computed independently. The choice of the *design velocity field* $\delta \boldsymbol{X}$ based on techniques of *computer aided geometric design* (CAGD) is seperated from details of the finite element description.

Computational benefits

Different strategies to generate the desired gradients are available as discussed above. A comparison of computational schemes based on *continuous variations* versus *discrete analytical derivatives* as characterised in Figure 2 has been investigated in [5]. The superior computational behaviour of the advocated variational approach has been proven. The benefits are even more obvious in case of finite difference approximations of the desired (analytical) gradients.

Furthermore, *high performance computing* (HPC) techniques can be applied most efficiently if the underlying theory already guarantees an optimised computational approach. The benefits are summarised by the already mentioned phrase *There is nothing so practical as a good theory* [9].

Design space exploration

The sensitivity matrix $\boldsymbol{S} = -\boldsymbol{K}^{-1}\boldsymbol{P}$ is computable and offers the chance to investigate its *internal structure* using the *singular value decomposition* (SVD). Based upon this insight, the design space can be reduced to the most significant design modes with highest impact on structural response, see [6, 7].

The real matrix $\boldsymbol{S}$ of order $m \times n$ can be factorised using the *singular value decomposition* (SVD) as follows

$$\boldsymbol{S} = \boldsymbol{Y}\,\boldsymbol{\Sigma}\,\boldsymbol{Z}^T = \sum_{i=1}^{\min(m,n)} \sigma_{ii}\, \mathbf{y}_i\, \mathbf{z}_i^T. \qquad (13)$$

The square matrix $\boldsymbol{Y}$ of order $m \times m$ contains the orthonormal system of physical *left singular vectors* $\mathbf{y}_i$ describing the structural response modes. The square matrix $\boldsymbol{Z}$ of order $n \times n$ contains the orthonormal system of geometrical *right singular vectors*, i.e. the design modes $\mathbf{z}_i$. The diagonal matrix $\boldsymbol{\Sigma}$ of order $m \times n$ contains the positive singular values σ_{ii} in decreasing order.

Inserting Eq. (13) into Eq. (12) yields

$$\delta f_{ij} = \left(\boldsymbol{b}_i^{\mathrm{T}} + \boldsymbol{c}_i^{\mathrm{T}}\, \boldsymbol{Y}\,\boldsymbol{\Sigma}\,\boldsymbol{Z}^T\right)\, \delta \boldsymbol{X}_j. \qquad (14)$$

This relationship can be further reformulated, e.g. $\boldsymbol{Z}^T \delta \boldsymbol{X}_j$ measures the impact of design modifications on the structural response. Overall, the results are used to explore the design space and to perform *what-if analyses* in order to evaluate the effect of design modifications on different objective and constraint functions.

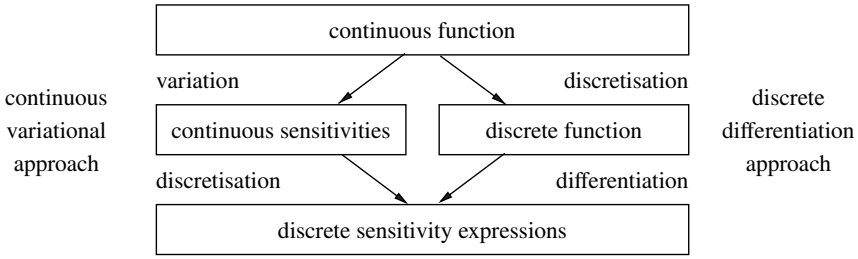

Figure 2: Order of steps within variational and analytical sensitivity analysis.

Multiscale structural optimisation

An intensive introduction and detailed explanations of methods for multiscale structural analysis are given in [12, 13, 14, 15]. Commonly, the homogenised stress and material tensors are deduced from an averaged potential energy of the microstructure by partial derivatives with respect to the macroscopic deformation gradient. Multiscale structural optimisation is fully explored in [8].

A typical multiscale structural optimisation procedure contains the definition of the model problem with the initial designs on different scales, objective functions (OF), constraints (CON) and design parameters (DP), MSA for the stated boundary value problem (BVP), a multiscale design sensitivity analysis (DSA) based on the obtained multiscale solution and an iterative determination of design parameter updates based on non-linear programming algorithms (NLP). The aforementioned sequence of steps is illustrated in Figure 3. It is emphasised that constraints and design parameters can be defined on different length scales and diverse combinations are possible. Additionally, different types of design parameters on the macroscale $\overline{\boldsymbol{\mathcal{K}}}$ and the microscale $\boldsymbol{\mathcal{K}}$ can be chosen. Beside material parameters in general, dimensions of parts, topological changes as well as changes of the shape are often referred. The design parameters in the following illustrative example are based on geometrical properties of control points within methods for computer aided geometric design (CAGD) or morphing based design parametrisation techniques.

The design sensitivity analysis part contains the evaluation of sensitivity information for a stated mechanical system and allows to answer the following questions: *How will physical responses in* $\overline{\boldsymbol{\mathcal{K}}}$ *react, if design parameters either only in* $\overline{\boldsymbol{\mathcal{K}}}$*, or only in* $\boldsymbol{\mathcal{K}}$*, or both in* $\overline{\boldsymbol{\mathcal{K}}}$ *and* $\boldsymbol{\mathcal{K}}$ *change?*

The answers for these questions come along with predictions for changes of the overall mechanical behaviour due to changes of design parameters on different length scales. Due to the fact that the MSA part might become time consuming, the major focus lies on the provision of efficient methods for DSA. Despite the overhead on theory and analytical calculus, the variational approach is beneficial in terms of improved and convenient computation times. An accurate numerical implementation leads to time consumptions for one MSA and one DSA in a similar range.

A further improvement can be gained by the application of mentioned HPC and common parallelisation techniques. Within MSA, the solution of each microscopic boundary value problem in each individual macroscopic integration point contributes to the overall macroscopic residual and stiffness operators. In a similar way, the determination of sensitivity information can be performed for each microscopic boundary value problem in each macroscopic integration point separately and each individual contribution is assembled to the overall macroscopic pseudo load operator.

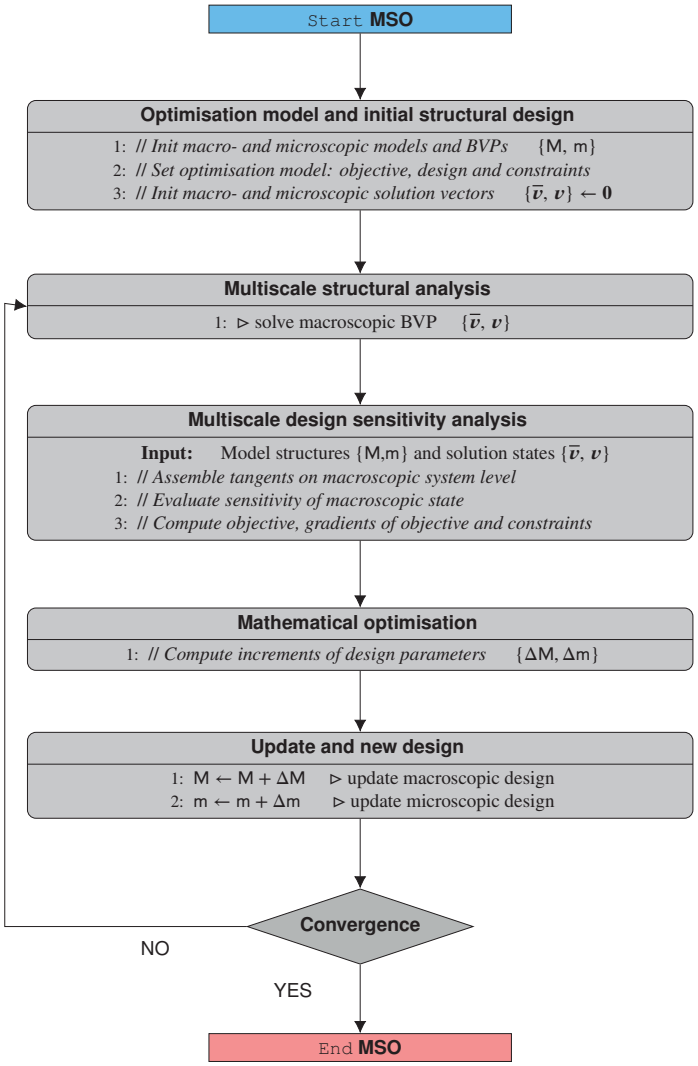

Figure 3: Framework for multiscale structural optimisation (MSO).

Multiscale design sensitivity analysis

For the formulation of accurate design sensitivity relations over multiple scales it is important to figure out correct dependencies. Generally, all functions depend on the macroscopic design and state parameters $\overline{\mathbf{X}}$ and $\overline{\mathbf{u}}$ as well as on the microscopic design and state parameters $\mathbf{X}$ and $\mathbf{u}$. This dependency is abbreviated by $(\cdot)$ for simplicity. Similar to formulations on single scales, multiscale analysis and multiscale optimisation are based on a general non-linear residual, i.e. $\overline{R}(\cdot;\overline{\boldsymbol{\eta}}) = 0$, with test function $\overline{\boldsymbol{\eta}}$. Despite design changes, the equilibrium state has to remain fulfilled and therefore the following variation of the macroscopic residual with respect to all design and state parameters can be stated

$$\delta\overline{R} = \delta_{\overline{X}}\overline{R} + \delta_{\overline{u}}\overline{R} + \delta_{X}\overline{R} + \delta_{u}\overline{R}. \quad (15)$$

Here, the introduced quantities are labelled as the macroscopic pseudo load operator $\overline{p}(\cdot;\overline{\boldsymbol{\eta}},\delta\overline{\mathbf{X}})$, the macroscopic physical stiffness operator $\overline{k}(\cdot;\overline{\boldsymbol{\eta}},\delta\overline{\mathbf{u}})$, the *multilevel* pseudo load operator $\widetilde{p}(\cdot;\overline{\boldsymbol{\eta}},\delta\mathbf{X})$ and the *multilevel* stiffness operator $\widetilde{k}(\cdot;\overline{\boldsymbol{\eta}},\delta\mathbf{u})$. The term *multilevel* indicates variations of the macroscopic residual $\overline{R}$ with respect to microscopic state and design parameters.

Analogous to formulations on single scales, the variation of the discrete residual reads

$$\begin{aligned}\delta\overline{\boldsymbol{R}} = \overline{\boldsymbol{P}}\delta\overline{\boldsymbol{X}} + \overline{\boldsymbol{K}}\delta\overline{\boldsymbol{U}} \\ + \widetilde{\boldsymbol{P}}\delta\boldsymbol{X} + \widetilde{\boldsymbol{K}}\delta\boldsymbol{U} = \boldsymbol{0}.\end{aligned} \quad (16)$$

The introduced matrices are identified as the macroscopic pseudo load $\overline{\boldsymbol{P}}$, the macroscopic physical stiffness $\overline{\boldsymbol{K}}$, the *multilevel* pseudo load $\widetilde{\boldsymbol{P}}$ and the *multilevel* stiffness $\widetilde{\boldsymbol{K}}$, respectively. The discrete sensitivity of the macroscopic state consists of two parts

$$\delta\overline{\boldsymbol{U}} = \overline{\boldsymbol{S}}\,\delta\overline{\boldsymbol{X}} + \widetilde{\boldsymbol{S}}\,\delta\boldsymbol{X}. \quad (17)$$

The macroscopic sensitivity matrix $\overline{\boldsymbol{S}} = -\overline{\boldsymbol{K}}^{-1}\overline{\boldsymbol{P}}$ incorporates any macroscopic design variation $\delta\overline{\boldsymbol{X}}$. Additionally, the effect of any microscopic design variation $\delta\boldsymbol{X}$ is given by the multilevel sensitivity matrix $\widetilde{\boldsymbol{S}} = -\overline{\boldsymbol{K}}^{-1}\left(\widetilde{\boldsymbol{K}}\,\boldsymbol{S} + \widetilde{\boldsymbol{P}}\right)$, where the sensitivity of the microscopic state $\boldsymbol{S} = -\boldsymbol{K}^{-1}\boldsymbol{P}$ is included.

Finally, an overall sensitivity relation for an arbitrary functional $f(\overline{\boldsymbol{X}},\overline{\boldsymbol{U}},\boldsymbol{X},\boldsymbol{U})$ can be obtained

$$\begin{aligned}\delta f = \left(\frac{\partial f}{\partial\overline{\boldsymbol{X}}} + \frac{\partial f}{\partial\overline{\boldsymbol{U}}}\,\overline{\boldsymbol{S}}\right)\delta\overline{\boldsymbol{X}} \\ + \left(\frac{\partial f}{\partial\boldsymbol{X}} + \frac{\partial f}{\partial\overline{\boldsymbol{U}}}\,\widetilde{\boldsymbol{S}} + \frac{\partial f}{\partial\boldsymbol{U}}\,\boldsymbol{S}\right)\delta\boldsymbol{X}.\end{aligned} \quad (18)$$

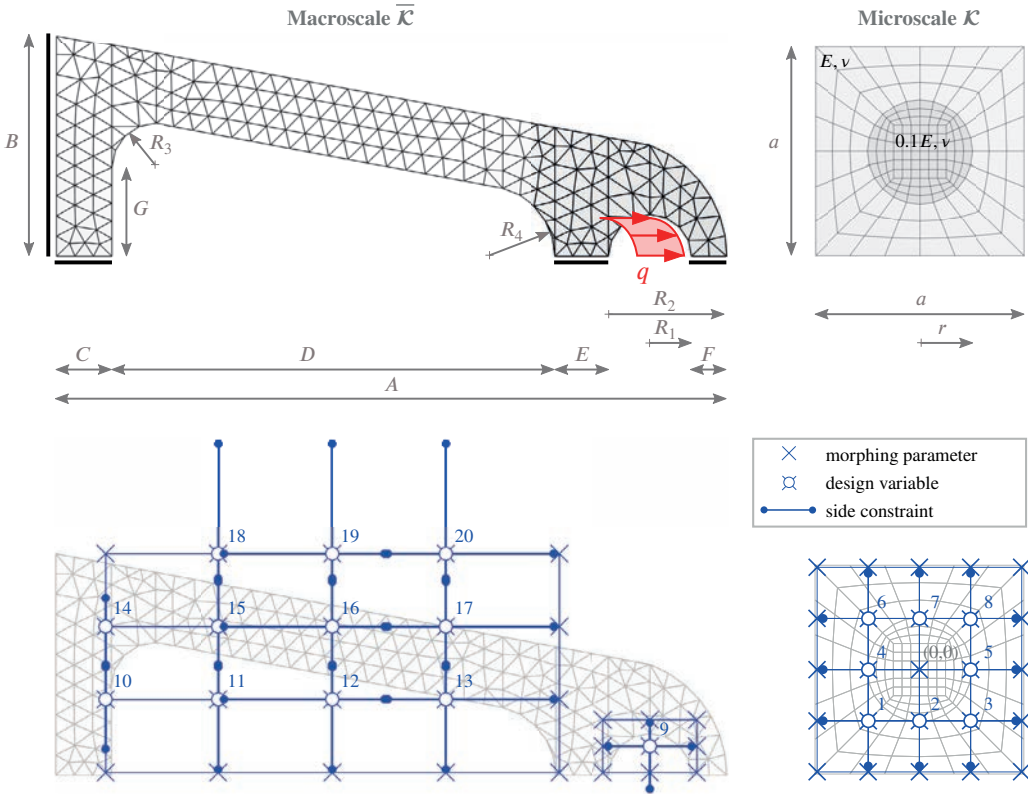

Figure 4: Mechanical system and FE mesh for the macro- and microscopic initial design (top line). Optimisation model for macroscale with two morphing boxes and for microscale with one morphing box (bottom line).

Numerical investigation

The following numerical investigation briefly sketches the multiscale optimisation of a macroscopic bracket, see [8] for complete information. The underlying microscale representation contains a stiff matrix material and a softer inclusion. The mechanical system is illustrated in Figure 4. The performance of the initial macroscopic system in terms of the displacements is illustrated in Figure 6.

The target is to minimise the overall macroscopic compliance $\overline{C}$ by modification of design parameters on the macro- and the microscale. This task is equivalent to the maximisation of the overall macroscopic stiffness. The defined constraints refer the individual volumes of the systems, which have to remain constant during the optimisation process but especially in the solution point.

The design parametrisation is based on so-called morphing techniques, where the coordinates of the control points of the morphing boxes are incorporated as design parameters, see Figure 4. The advantage of morphing based design parametrisation is its applicability to arbitrary FE meshes with diverse element formulations.

The design sensitivity information is firstly obtained with respect to the nodal coordinates of the FE mesh. Afterwards, these results have to be transformed to the chosen design space using so-called design velocity fields.

The *sequential quadratic programming* (SQP) method has been used for optimisation. It takes 23 iterations to find a feasible solution and to reduce the value of the objective by 17% , i.e. $\overline{C}^{\,\mathrm{opt}} / \overline{C}^{\,\mathrm{ini}} = 0.329 / 0.398 = 0.83$.

The distribution of design parameters for the optimal design is shown in Figure 5. The results obtained for one half of the system can be mirrored due to symmetry to the design of the overall system. The performance of the macroscopic system in terms of the displacements is illustrated in Figure 6 and proves that the stiffness is increased due to the fact that the resulting displacements reduce.

The example demonstrates the possibility to incorporate microscopic design parameters and constraints into the overall macroscopic optimisation process. Thus, multiscale optimisation problems based on variational design sensitivity analysis can be solved with convenient computation times.

Comment on computation times

The computation time for the solution of the overall optimisation problem reads 245 minutes and as already mentioned 23 iterations are required. That means that on average about 10 minutes per iteration are needed for the defined optimisation model with 1089 macroscopic integration points (which corresponds the number of microscopic BVP solutions), 363 finite elements and 464 degrees of freedom on the macroscale, and 180 finite elements and 386 degrees of freedom on the microscale. The computations are carried out on a mobile workstation with an Intel® Core™ i7-4800MQ CPU and 32 GB of RAM. Beside a discussion on benefits, a detailed exploration of computation efforts for the solution of several optimisation problems based on the variational approach for sensitivity analysis and the finite differences methods (numerical determination of gradients) can be found in [8]. It can be assumed that choosing a different and a more performant hardware environment together with some code optimisation steps would lead to more performant computation times and faster solution processes, but the ratio between variational and numerical computation of gradients remains equal.

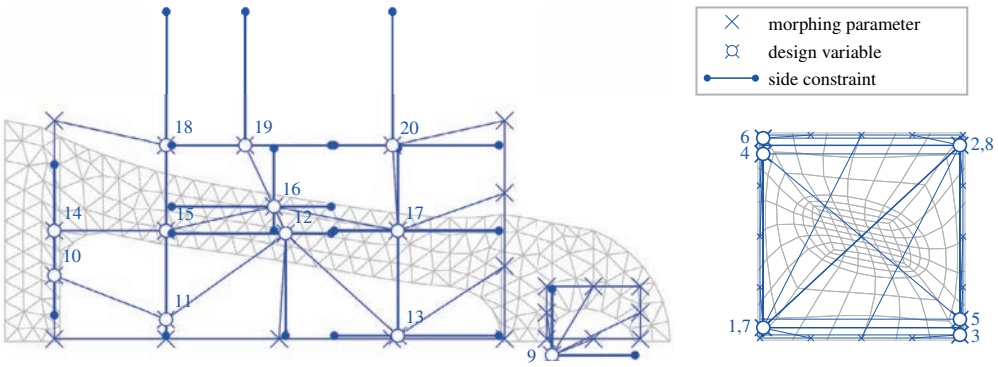

Figure 5: Distribution of design parameters after optimisation: macro design (left) and micro design (right).

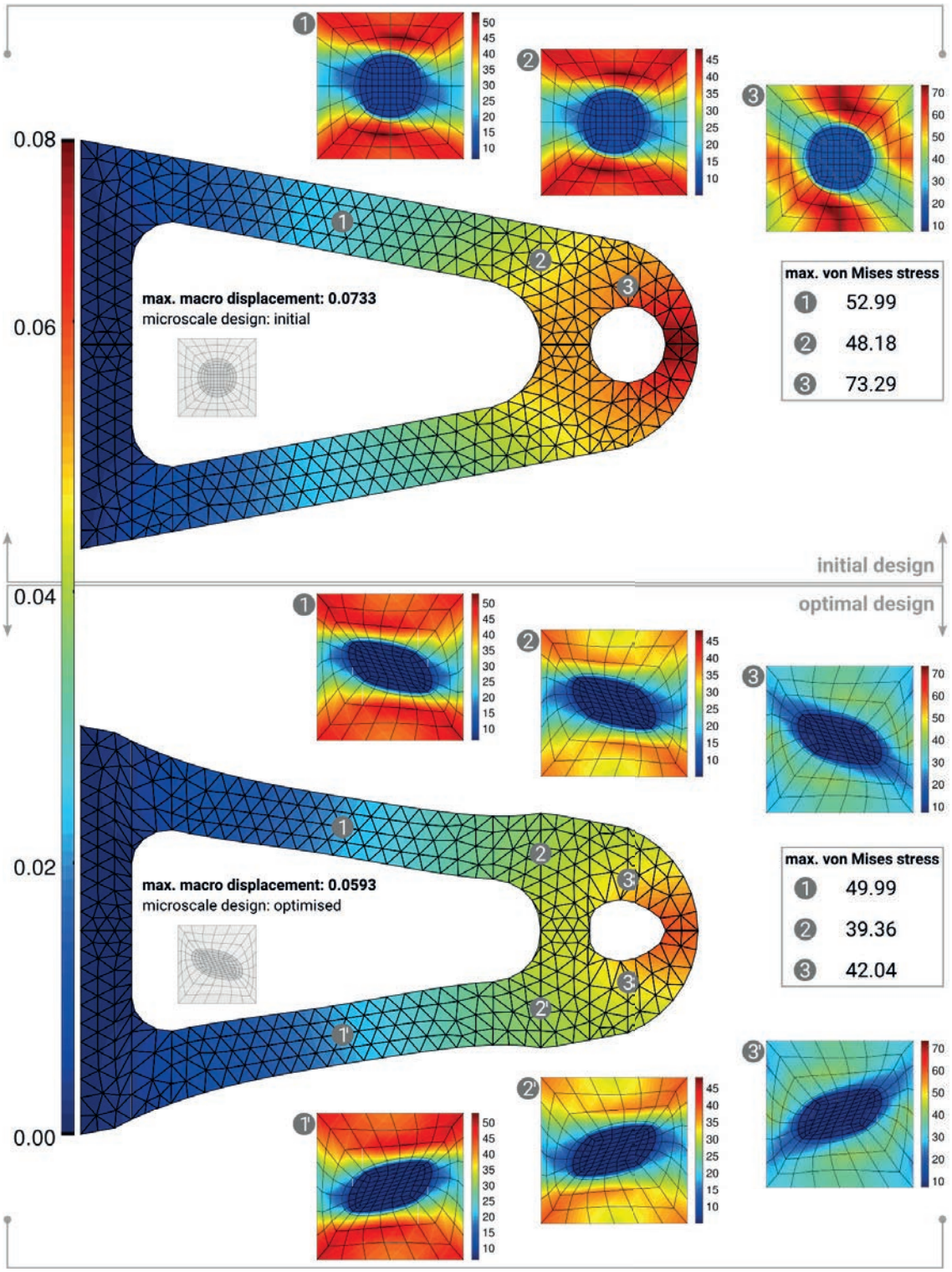

Figure 6: Multiscale optimisation of a bracket: macroscopic displacements (large) for initial and optimised supplemented designs. Microscopic von Mises stress distribution in selected macroscopic integration points (1-3) for initial and optimised design. Due to symmetry, microstructures can be copied to design the full system.

Conclusion

The variational approach to design sensitivity analysis of nonlinear mechanical problems has been outlined briefly indicating the central theoretical concepts. Furthermore, the corresponding structure of its application to multiscale problems has been sketched. An illustrative example shows the applicability of the derived optimisation algorithm with objective and constraint functions as well as design parameters from both scales.

References

[1] J. Arora. An exposition of the material derivative approach for structural shape sensitivity analysis. *Comput Methods Appl Mech Eng*, 105:41–62, 1993.

[2] F.-J. Barthold. *Zur Kontinuumsmechanik inverser Geometrieprobleme*. Habilitation, Braunschweiger Schriften zur Mechanik 44-2002, TU Braunschweig, 2002.

[3] F.-J. Barthold. Remarks on variational shape sensitivity analysis based on local coordinates. *Eng Anal Bound Elem*, 32(11):971–985, 2008.

[4] F.-J. Barthold and E. Stein. A continuum mechanical based formulation of the variational sensitivity analysis in structural optimization. Part I: Analysis. *Struct Optim*, 11 (1/2):29–42, 1996.

[5] F.-J. Barthold, N. Gerzen, W. Kijanski, and D. Materna. Efficient variational design sensitivity analysis. In P. Neittaanmäki, S. Repin, and T. Tuovinen, editors, *Mathematical Modeling and Optimization of Complex Structures*, Cham, 2016. Springer Int. Publ.

[6] N. Gerzen. *Analysis and Applications of Variational Sensitivity Information in Structural Optimisation*. Shaker Verlag, Düren, 2014.

[7] N. Gerzen, D. Materna, and F.-J. Barthold. The inner structure of sensitivities in nodal based shape optimisation. *Comp Mech*, 49: 379–396, 2012.

[8] W. Kijanski. *Optimal Material Design based on Variational Sensitivity Analysis*. PhD Thesis, TU Dortmund, 2018.

[9] M. H. Kuhn. Lewin, Kurt. Field Theory of Social Science: Selected Theoretical Papers. *Ann Am Acad Pol Soc Sci*, 276(1):146–147, 1951.

[10] D. Materna. *Structural and Sensitivity Analysis for the Primal and Dual Problems in the Physical and Material Spaces*. Shaker Verlag, Düren, 2010.

[11] D. Materna and F.-J. Barthold. Theoretical aspects and applications of variational sensitivity analysis in the physical and material space. In R. F. Linton and T. B. Carroll, editors, *Computational Optimization: New Research Developments*, pages 397–444, Hauppauge, 2010. Nova Science Publishers.

[12] C. Miehe. Strain-driven homogenization of inelastic microstructures and composites based on an incremental variational formulation. *Int J Numer Meth Eng*, 55(11):1285–1322, 2002.

[13] C. Miehe. Computational micro-to-macro transitions for discretized microstructures of heterogeneous materials at finite strains based on the minimization of averaged incremental energy. *Comput Methods Appl Mech Eng*, 192(5–6):559–591, 2003.

[14] C. Miehe and C. Bayreuther. On multiscale fe analyses of heterogeneous structures: from homogenization to multigrid solvers. *Int J Numer Meth Eng*, 71(10):1135–1180, 2007.

[15] J. Schröder. A numerical two-scale homogenization scheme: the fe^2-method. In J. Schröder and K. Hackl, editors, *Plasticity and Beyond*, volume 550 of *CISM*, pages 1–64. Springer Vienna, 2014.

[16] D. Tortorelli and Z. Wang. A systematic approach to shape sensitivity analysis. *Int J Solids Struct*, 30(9):1181–1212, 1993.

In Memoriam Erwin Stein (1931 – 2018)

by Walter Wunderlich[1]

[1]Chair of Structural Analysis, Technical University of Munich, Germany

Figure 1: Erwin Stein (1931 - 2018).

On December 19, 2018, Erwin Stein, my colleague and friend for 60 years, died at the age of 87. Only two weeks earlier, he was still in a normal shape, but very worried about the critical health situation of his wife Gisela. Then, she unexpectedly informed me that Erwin had passed away after some days of sudden unconsciousness, which had overtaken him late in the night of December 13 after working at his desk.

With Erwin Stein the community of Computational Mechanics is losing a nationally and internationally highly renowned scientist, and the German Association of Computational Mechanics one of its founders and honorary presidents.

Erwin Stein was born on July 5, 1931 in Altendiez/ Lahn. After his highschool finals, he studied from 1951 at the Technische Hochschule Darmstadt taking courses mainly in civil engineering but also in mathematics.

During this time he got married to Gisela in 1953 and the two daughters Ulrike and Annelie were born, later followed by their son Matthias. After obtaining his diploma in civil engineering in 1958, Erwin Stein took his first position in the consulting firm for bridge engineering Dr. Homberg in Hagen/Westfalen where we both met for the first time and became friends. Whereas my work in this company lasted for about three years, Erwin left after one year and started his scientific career.

In 1959, he accepted an offer by Prof. Bornscheuer of the University of Stuttgart to become an assistent at the Institut für Baustatik, where he worked with great commitment for about 12 years, from 1965 as "Oberingenieur". In this time, the computer based methods of structural mechanics came into the focus of research. With enthusiasm, Erwin followed this new field leading in 1964 to his dissertation on "Die Trefftz-Methode für Balken, Platten und Schalen" and in 1969 to his "Habilitation" and the venia legendi for "Baustatik und Baumechanik".

In recognition of his abilities, he became spokesperson ("Sprecher") of the new and distinguished Collaborative Research Centre SFB 64 (Lightweight Structures) of the German Research Foundation (DFG). In the same year (1970) he also was organizer of a seminar in Stuttgart in which results of various DFG-projects using computer-oriented methods were discussed. The corresponding presentations were published in the book "Finite Elemente in der Statik" and give an overview about the status of developments in this field in that early stage.

The main part of the academic career of Erwin Stein is connected with the University of Hannover, however. In the year 1971, he accepted a call to the chair of "Baumechanik" at the Department of Civil Engineering of the Technische Universität Hannover as successor of Professor Theodor Lehmann. He remained there until his retirement in 1998 and even beyond as Emeritus another 20 years, in which he worked as hard as before.

In this long period, Erwin Stein formed an institute of high national and international reputation. With his

team, he achieved substantial progress in the field of Computational Mechanics, especially in computational structural and solid mechanics and became well-known for the profound quality of his research. He worked in wide-spread research areas, from basic theoretical formulations to numerical realization and practical applications. On the one hand, he accentuated practical problems of analysis and design, the latter influenced by his license as Proof-Engineer (Prüfingenieur) which he obtained in 1975. On the other hand, he emphasized the importance of mathematics and enforced the collaboration with applied mathematicians. The broad spectrum and the development of his research are reflected in his numerous papers (more than 300) in highly ranked journals, books, and conference contributions. He was editor or coeditor of many books, journals and proceedings, including the Encyclopedia of Computational Mechanics.

Erwin Stein promoted the practical application of the finite element method already at its early stages, e.g. in Germany organizing the conference series "Finite Elemente in der Baupraxis" together with me, and hosted the first one in 1978 in Hannover. In addition, he emphasized the theoretical development, e.g. by founding the working group "Diskretisierende Methoden in der Strukturmechanik" within the International Association of Applied Mathematics and Mechanics (GAMM), and organizing workshops at the research centers in Bad Honnef and Oberwolfach. In the framework of the German Research Foundation, in 1981, he initiated the nationwide Special Research Program "Nichtlineare Berechnungen in der Strukturmechanik" and worked on about 50 other research projects.

In his teaching responsibilities Erwin Stein successfully educated in his profound manner students of civil engineering for 27 years in the basics of mechanics as well as in advanced courses (Fig. 2). Quoting himself from one of his papers: "Structural engineers need ingenium - this Latin word means imagination, rational thinking, talents for theoria cum praxi, (natural) determination ...-" gives some of the motivation about his teaching approach. Sometimes even some philosophical notes were added to the often demanding contents of his lectures.

With his enthusiasm he managed to attract the top students to his institute and formed a highly qualified team of scientists, the so-called "Stein-School". Many of his coworkers became professors at various universities expanding his ideas, and their institutes in turn developing to recognized centers of excellent research in many areas of computational mechanics.

Erwin Stein established and maintained a worldwide network. He was one of the founders of the International Association of Computational Mechanics (IACM) as well as of the German Association of Computational Mechanics (GACM). With his dedicated commitment he contributed essentially to the development of these and related organizations, like ECCM (European Conference on Computional Mechanics) and Dekomech (Deutsches Komitee für Mechanik). He was a regular participant in national and international congresses, often giving invited or plenary lectures, always on a sophisticated level.

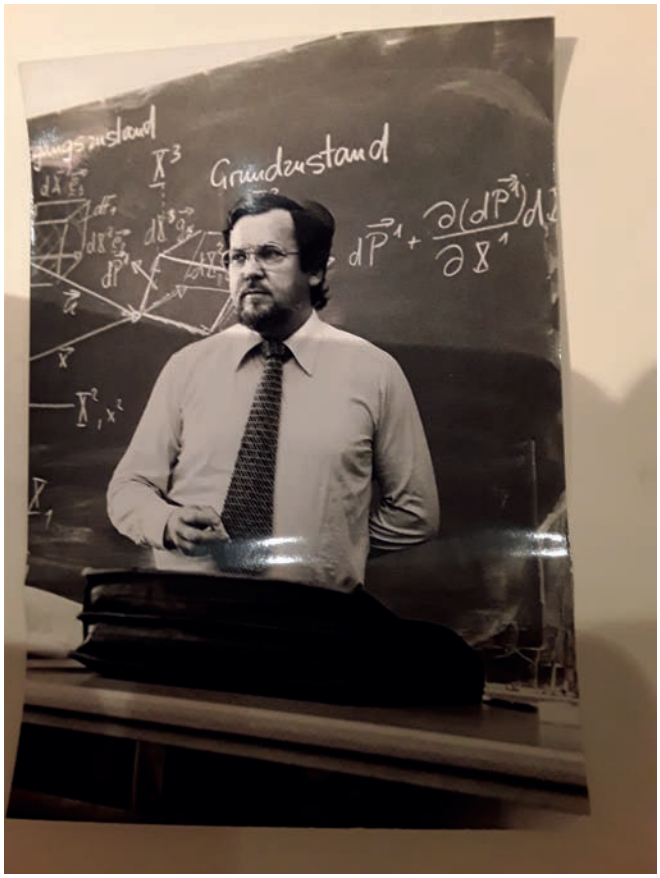

Figure 2: Teaching at the University of Hannover.

As an exceptional contribution to the scientific community, his research about Gottfried Wilhelm Leibniz has to be emphasized. In the time of his retirement Erwin became more and more attracted by the person and the work of this last universal scholar. He even tried hard to read some of his contributions in the original Latin language. In particular, Leibniz' four species calculating machine (machina arithmetica 1698) and its mode of operation was the focus of the investigations, which

he improved by a new construction built together with the mechanical engineer F.O. Kopp. With this and other rebuilt machines of Leibniz, he formed an exhibition at the University of Hannover (in 2006 renamed Gottfried Wilhelm Leibniz Universität Hannover) which was also shown at several other universities and places.

Moreover, he expanded his research interest into other areas of Leibniz's work: mathematics, mechanics, philosophy, theology, and others. Several publications describe his impressive research work, especially his last book: "Der Universalgelehrte Gottfried Wilhelm Leibniz" - edited together with A. von Boetticher - includes several chapters of the recent Leibniz-research of Erwin. Until his last days he became inspired by looking at the bust of Leibniz, which was placed in the garden of his house. On many occasions he praised the work and ideas of this great scientist, as in his last lecture given at the GAMM Annual Meeting in Munich in March 2018 (Fig. 3).

In 2011, he was awarded the "Verdienstkreuz 1. Klasse des Niedersächsischen Verdienstordens", in appreciation of special efforts in science and research and his accomplishments for the inheritance of Leibniz.

In recognition of his academic merits, Erwin Stein also received an honorary doctorate (Dr.-Ing. E.h.) from the University of Stuttgart (in 1986), and three honorary degrees (Dr. h.c.) from the universities of St. Petersburg, Xuzhou, and Posen. Several other awards followed, among them, as the most prominent ones, the Gauß-Newton Medal of the International Association for Computational Mechanics (IACM) and the Ritz-Galerkin Medal of the European Community on Computational Methods in Applied Sciences (ECCOMAS). He was honorary member of several scientific organizations and honorary president of the GACM.

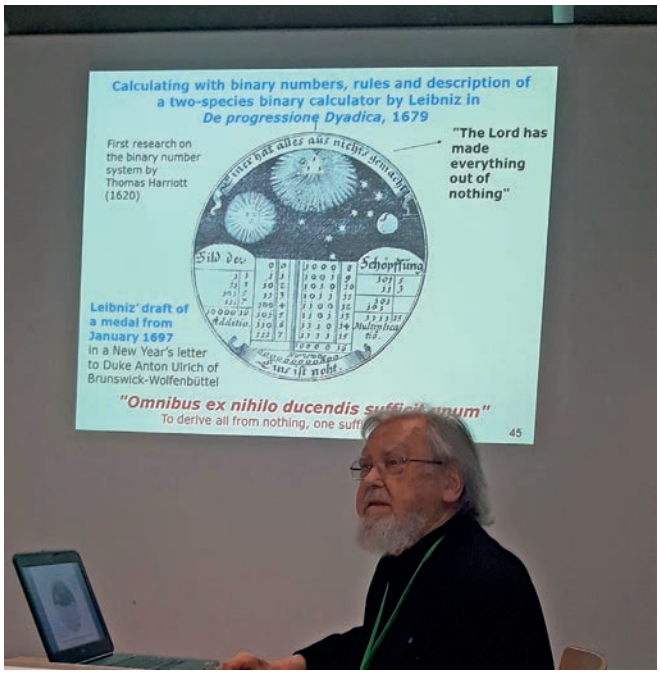

Figure 3: At the GAMM-Meeting in Munich 2018.

The community of Computational Mechanics is grateful for his achievements and impulses and will cherish his scientific legacy.

Erwin Stein was an exceptional scientist and a great personality. We mourn his loss and express our sorrow and sympathy to his wife Gisela und his children. His presence will be missed but our memories of him and of his friendship will remain.

Selected Conference Announcements

The following three selected conferences are jointly prepared together with GACM to support the local organizations. For an up-to date general conference schedule, please also visit the GACM website at www.gacm.de/activities.

8th ECCOMAS Congress & 14th WCCM 2020

The 8th ECCOMAS Congress 2020 jointly organized with the 14th IACM World Congress on Computational Mechanics will be held in Paris, France, July 19 - 24, 2020.

AfriComp 2020/SACAM 2020

The African Conference on Computational Mechanics jointly organized with the South African Conference on Computational and Applied Mechanics will take place in Cape Town, South Africa, November 30 - December 02, 2020.

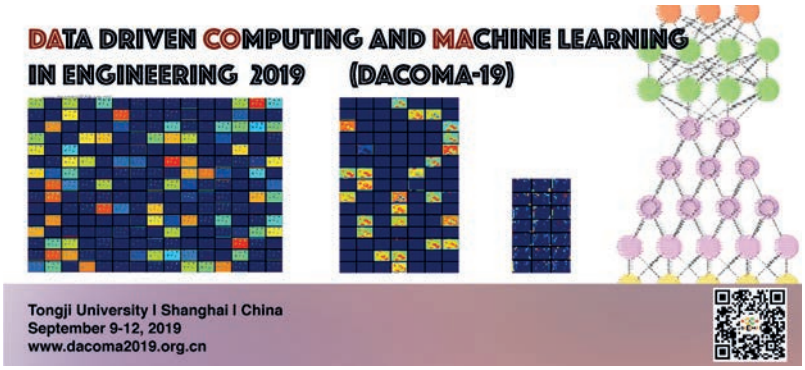

DACOMA-19

The conference on Data Driven Computing and Machine Learning in Engineering will be held in Shanghai, China, September 09 - 12, 2019.

Notes:

Notes:

Notes:

gacm German Association for Computational Mechanics

the german association for computational mechanics

Institut für Statik und Dynamik der Tragwerke
Technische Universität Dresden
01062 Dresden
Phone: +49 351-463-35738
Fax: +49 351-463-37086
email: gacm@mailbox.tu-dresden.de
Internet: www.gacm.de